DOI 10.1016/j.jconrel.2023.10.014

The alpha-adrenergic antagonist prazosin promotes cytosolic siRNA delivery from lysosomal compartments

Thijs Van de Vyver[1]; Cristina Muntean[1,3]; Iuliia Efimova[2,3]; Dmitri V. Krysko[2,3,4]; Lynn De Backer[1]; Stefaan C. De Smedt[1]; Koen Raemdonck[1,3,*]

[1] Ghent Research Group on Nanomedicines, Laboratory of General Biochemistry and Physical Pharmacy, Faculty of Pharmaceutical Sciences, Ghent University, Ottergemsesteenweg 460, 9000 Ghent, Belgium

thijs.vandevyver@gmail.com

cristina.muntean@ugent.be

lynn.debacker@ugent.be

stefaan.desmedt@ugent.be

koen.raemdonck@ugent.be

[2] Cell Death Investigation and Therapy Laboratory, Department of Human Structure and Repair, Faculty of Medicine and Health Sciences, Ghent University, 9000 Ghent, Belgium;

iuliia.efimova@ugent.be

dmitri.krysko@ugent.be

[3] Cancer Research Institute Ghent, 9000 Ghent, Belgium

[4] Department of Pathophysiology, Sechenov First Moscow State Medical University (Sechenov University), 119146 Moscow, Russia

* Corresponding author: Prof. Koen Raemdonck

koen.raemdonck@ugent.be

ABSTRACT

The widespread use of small interfering RNA (siRNA) is limited by the multiple extra- and intracellular barriers upon *in vivo* administration. Hence, suitable delivery systems, based on siRNA encapsulation in nanoparticles or its conjugation to targeting ligands, have been developed. Nevertheless, at the intracellular level, these state-of-the-art delivery systems still suffer from a low endosomal escape efficiency. Consequently, the bulk of the endocytosed siRNA drug rapidly accumulates in the lysosomal compartment. We recently reported that a wide variety of cationic amphiphilic drugs (CADs) can promote small nucleic acid delivery from the endolysosomal compartment into the cytosol *via* transient induction of lysosomal membrane permeabilization. Here, we describe the identification of alternate siRNA delivery enhancers from the NIH Clinical Compound Collection that do not have the typical physicochemical properties of CADs. Additionally, we demonstrate improved endolysosomal escape of siRNA via a cholesterol conjugate and polymeric carriers with the α1-adrenergic antagonist prazosin, which was identified as the best performing delivery enhancer from the compound screen. A more detailed assessment of the mode-of-action of prazosin suggests that a different cellular phenotype compared to typical CAD adjuvants drives cytosolic siRNA delivery. As it has been described in the literature that prazosin also induces cancer cell apoptosis and promotes antigen cross-presentation in dendritic cells, the proof-of-concept data in this work provides opportunities for the repurposing of prazosin in an anti-cancer combination strategy with siRNA.

KEYWORDS: drug repurposing; cationic amphiphilic drugs; lysosomal membrane permeabilization; endosomal escape; combination therapy; cancer therapy; cancer immunotherapy

GRAPHICAL ABSTRACT

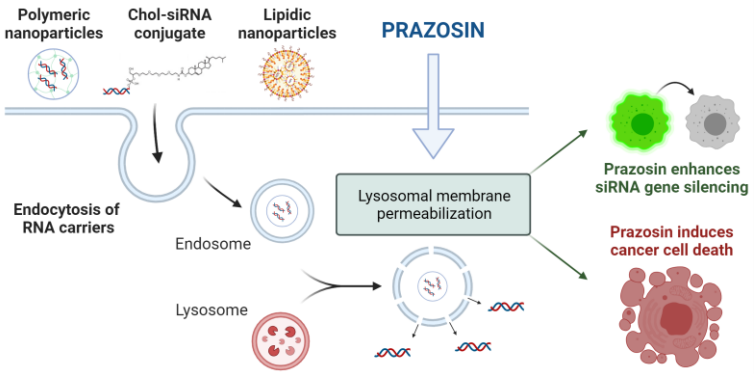

1. INTRODUCTION

Post-transcriptional gene silencing by small interfering RNA (siRNA) shows great promise for the treatment of any type of human pathology with a recognized (over)expression of one or more disease-causing genes[1–3]. Since the discovery of the RNA interference (RNAi) mechanism more than 2 decades ago[4], considerable efforts have been made to identify suitable carrier systems that can effectively and safely deliver siRNA drugs to target cells[2,3]. At the intracellular level, siRNAs need to access the cytosol to activate the RNAi machinery and induce sequence-specific mRNA degradation[3,5,6]. While multiple delivery strategies are under investigation, lipid nanoparticles (LNPs) and conjugates are the most advanced siRNA delivery technologies to date, as exemplified by the recent clinical approval of patisiran (siRNA-loaded LNPs) and givosiran/lumasiran/inclisiran/vutrisiran (N-acetylgalactosamine (GalNAc)-siRNA conjugates)[7–10]. However, cytosolic delivery remains relatively inefficient as endocytic uptake of LNPs and conjugates results in endosomal sequestration[5,11–13] and finally lysosomal degradation[14–19]. Since only a minor fraction (i.e. 1-2% in case of LNPs[17,18] and estimated < 0.01% in case of GalNAc-siRNA conjugates[3,13,20]) of the internalized siRNA dose escapes into the cytosol during this rapid trafficking process, endosomal escape remains a major bottleneck[5,17,18,21,22].

Interestingly, growing evidence suggests that both the extra- and intracellular barriers for nucleic acid delivery can in part be overcome by the application of distinct classes of small molecule drugs[22–24]. We recently reported that structurally and pharmacologically diverse cationic amphiphilic drugs (CADs) can be repurposed as siRNA delivery enhancers when applied in a sequential manner to siRNA-transfected cells[25–27]. CADs are known to mainly accumulate in lysosomes upon exposure to cells *via* a well-known pH-dependent ion trapping mechanism, leading to functional inhibition of the lysosomal acid sphingomyelinase[28,29], phospholipidosis (PLD)[30,31], lysosomal swelling[32,33] and lysosomal membrane permeabilization (LMP)[34,35]. CAD-induced LMP is actively being explored as a means to selectively kill cancer cells via so-called lysosomal cell death[34,35]. However, it was demonstrated by Joris *et al.* that some CADs (*e.g.*, the anti-histaminic compound desloratadine) can induce a transient and non-lethal LMP phenotype in non-small cell lung cancer (NSCLC) cells, which allowed dextran nanogel-encapsulated siRNA to diffuse from the lysosomal compartment into the cytosol[27]. Hence, in contrast to governing endosomal escape models, these data suggest that lysosomes are not necessarily a dead end for siRNA nanomedicines. In follow-up work, we established the broader applicability of CADs as

adjuvants for the delivery of both siRNA and antisense oligonucleotides in distinct cancer cell lines.[25] Additionally, we found that the CAD adjuvant approach is carrier-specific, as only nanomedicines that release a sufficient amount of uncomplexed siRNA inside the endolysosomal lumen allowed diffusion of siRNA through the CAD-induced pores in the limiting lysosomal membrane[25]. In an attempt to identify additional small molecules that could similarly enhance the gene silencing potential of siRNA-loaded nanogels in NSCLC cells, a drug repurposing screen was performed, exposing the transfected cells to the 'National Institutes of Health Clinical Collection' compound library (NIHCC, 700 compounds)[25]. This screen revealed a strong enrichment of both CADs and PLD inducers in the hit group, correlating the lysosomotropic properties of CADs with the induction of an acquired lysosomal storage disease phenotype and improved cytosolic siRNA delivery[27]. However, several hits from this compound screen did not comply with the applied CAD definition (calculated logP (clogP) > 3 and pKa1 > 6). In this work, we further describe these additional hit compounds and investigated the adjuvant activity of the α1-adrenergic receptor antagonist prazosin, the first ranked hit compound of the screen, in more detail. Our data revealed that prazosin, but not the structural quinazoline-analogues doxazosin or terazosin, can strongly promote the cytosolic delivery of cholesterol-conjugated or polymer-transfected siRNA in NSCLC cells. Importantly, prazosin treatment leads to lysosomal swelling and the appearance of cytoplasmic vacuoles while PLD induction was not observed, highlighting that prazosin induces a distinct cellular phenotype than CADs[25,27]. Additionally, we showed that several PIKfyve inhibitors, likewise known to generate vacuoles and enlarged lysosomes, could promote siRNA delivery, although to a much lower extent compared to prazosin and CADs. It is therefore hypothesized that besides lysosomal swelling and vacuolization, other yet unidentified cellular processes might contribute to prazosin-induced cytosolic siRNA delivery. Notably, previous work has shown that prazosin is able to induce apoptotic cell death in several cancer cell types, both *in vitro* and *in vivo*[36–45]. In addition, recent research demonstrated that prazosin can also be repurposed to increase, both *in vitro* and *in vivo*, dendritic cell cross-presentation of antigenic peptides to naïve $CD8^+$ T-cells[46], which is one of the main driving forces of anti-tumor immunity[46–48]. Consequently, our work proposes a combination cancer treatment exploiting prazosin to concurrently promote cancer cell death, intracellular siRNA delivery (*e.g.*, targeting specific oncogenes) and cross-presentation of tumor-associated antigens.

2. RESULTS AND DISCUSSION

NIHCC compound screen reveals several non-CAD siRNA delivery enhancers

Screening of the NIHCC compound library has previously identified 96 compounds that significantly enhance the gene silencing potential of siRNA-loaded dextran nanogels (siNGs) in non-small cell lung cancer cells stably expressing the enhanced green fluorescent protein (H1299-eGFP)[25]. The cells were transfected with siNGs, loaded with eGFP-targeting siRNA (sieGFP) or a negative control sequence (siCTRL) respectively, and subsequently incubated with the compounds (20 µM) for 20 h in complete cell culture medium. In the hit group, 56 compounds (*i.e.* 58%) adhered to the applied CAD definition (clogP > 3 and pKa1 > 6)[49]. However, 40 hit compounds (*i.e.* 42%) with diverging chemical structures and pharmacology could not be classified as CADs ('non-CAD hits', **Table S1**). Hence, the observed siRNA delivery-promoting effect of these compounds cannot readily be correlated to the induction of a PLD phenotype and disruption of the lysosomal membrane, as has been extensively described in the literature for CADs[25,27,30,31,34,35].

To shed light on the potential mode-of-action of these non-CAD delivery enhancers, we first screened for enriched annotated molecular targets of the latter compounds **(Figure 1A)**. Here, a series of common targets and/or drug classes could be distinguished. First, three L-type calcium channel blockers (CCBs) that share a dihydropyridine (DHP) structure (amlodipine, lacidipine and felodipine) were identified as hits. L-type CCBs with and without a DHP core have previously shown to boost the potency of cholesterol-conjugated, cell-penetrating asymmetric siRNAs (cp-asiRNAs) when used in a co-incubation protocol, albeit this effect was linked to the stimulation of endocytosis rather than cytosolic delivery[50]. Hence, as the compounds in our screen were added after siNG transfection and given that five other L-type CCBs (isradipine, nifedipine, nimodipine, nitrendipine, nisoldipine and diltiazem) were not identified as hits, the involvement of this process in our screen seems unlikely. Interestingly, publicly available transcriptomics data (Connectivity Map or CMap data set of the Broad Institute[51]) suggest that CCBs can induce a transcriptional response similar to PLD inducers, which may be linked to the role of calcium signalling in lysosomal function[52]. Moreover, amlodipine contains a side chain with a basic amino group (pKa1 = 9.45) and has lysosomotropic properties, albeit the clogP < 3. As such, amlodipine is a known functional inhibitor of the acid sphingomyelinase enzyme[29] and PLD inducer[31] and might thus have a similar mode-of-action as the previously discussed CADs. Secondly, a set of tubulin

polymerization inhibitors (vindesine, podophyllotoxin and the anthelminthics albendazole, mebendazole and flubendazole) and four steroids (19-norethindrone acetate, medroxyprogesterone 17-acetate, tibolone and megestrol acetate) were defined as hits. As endo(lyso)somal vesicles move through the cytosol *via* microtubules, disrupting this network might increase the intracellular residence time and the likelihood of endosomal escape[53–58]. On the other hand, several steroids have shown to promote the activity of nucleic acid drugs with a pleiotropic mode-of-action (*e.g.*, enhance cellular uptake, *etc.*)[24]. Next, some antineoplastic drugs (triptolide, mitoxantrone, dactinomycin and the thymidylate synthase inhibitors carmofur and 5-fluorouracil) emerged as hits, albeit their supporting effects on siRNA delivery were overall rather limited and could potentially be linked to their toxicity. Only four non-CAD compounds (*i.e.* ~10%) improved siRNA-mediated eGFP knockdown to > 50% relative to control, compared to almost 32% of CADs (**Figure 1B**). Hexachlorophene and oligomycin A, respectively an antiseptic[59] and a potent inhibitor of the mitochondrial ATP synthase[60], have not yet been described as drug repurposing candidates. On the other hand, the antifungal itraconazole has recently been shown to enhance liposomal pDNA and siRNA delivery[61]. The latter was suggested to occur *via* the known binding of itraconazole to the Niemann-Pick C1 (NPC1) protein[62,63] in the late endosomal/lysosomal membrane, which leads to a blocked intracellular cholesterol trafficking and hyper-accumulation of cholesterol in the late endosomes and lysosomes. In accordance to other studies that inhibited NPC1 *via* genetic[19] or pharmacological[64] means, the enhanced transfection could potentially be linked to an increased cellular retention of pDNA/siRNA as a consequence of reduced recycling of endocytosed nucleic acids out of the cell. Finally, although the adjuvant effect is generally lower in the non-CAD hit group, compared to the CAD hits (**Figure 1B**), the most effective hit prazosin, a quinazoline-based α1-adrenergic antagonist, is not a typical CAD. Although prazosin did strongly increase the cellular granularity, as indicated by the augmented side scatter (SSC) signal, in contrast to the CADs no correlation was found here between the SSC signal and improved knockdown within the total non-CAD group (**Figure 1C**)[25]. Nevertheless, the mean SSC signal in the 'non-CAD hit group' was still significantly higher compared to the 'non-CAD no hit group' (**Figure S1**). Interestingly, 2 structural analogues of prazosin, *i.e.* doxazosin and terazosin, were respectively a minor hit (27% additional eGFP silencing) and no hit. Given that the strongest adjuvant effect in this screen was obtained with prazosin, we next aimed to investigate the cellular phenotype of this compound in more detail.

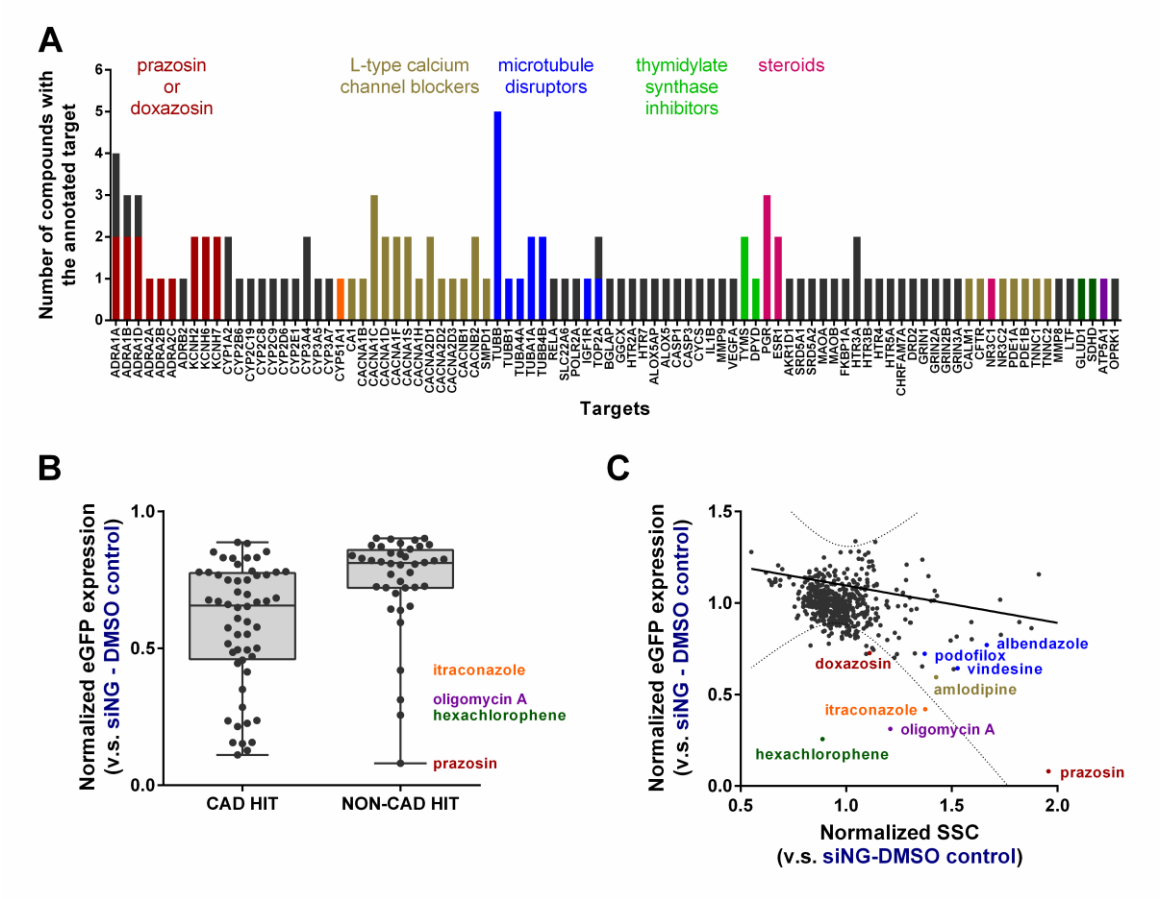

Figure 1. Next to CADs (clogP > 3 and pKa1 > 6), also non-CAD compounds were identified as siRNA delivery-promoting hits in the NIHCC library screen. (A) Summary of annotated targets for the siRNA delivery-promoting non-CAD compounds (*i.e.* 'non-CAD hits'). The abscissa indicates the documented protein targets of the non-CAD hits. The ordinate indicates the number of non-CAD hits that have each of the depicted proteins as a validated target according to the Drug Repurposing Hub database[65]. A summary of the annotated targets for each compound is provided in **Table S1**. **(B)** Box and whisker plot of the normalized eGFP expression (calculated % eGFP expression values of the individual compounds (20 µM, 20 h) were normalized to the siNG transfection alone (siNG-DMSO control) of each plate) of the 'CAD hit' (n = 56) and 'non-CAD hit' (n = 40) group. **(C)** Correlation between the side scatter (SSC) signal, normalized to the siNG-DMSO control of each plate, and the normalized eGFP expression (see above) in the group of all non-CADs (n = 572). The dashed line represents the 95% confidence band of the regression line (R^2 = 0.000207; ns). In both **(A)**, **(B)** and **(C)**, discussed compounds or drug classes are highlighted in associated colours. (eGFP = enhanced green fluorescent protein, NG = dex-HEMA nanogels, siNG = siRNA-loaded NG, NIHCC = National Institutes of Health Clinical Collection, CAD = cationic amphiphilic drug, siNG-DMSO control = siNG transfection in the absence of compound with equal amount of DMSO).

Secondary validation of quinazolinamine derivatives

To validate prazosin as a potent siRNA delivery enhancer, the compound and its structural analogues doxazosin and terazosin were subjected to secondary testing. Additionally, the previously identified CAD adjuvant desloratadine[25,27] was included as a benchmark (**Figure**

2A). Both prazosin and desloratadine evoked a clear concentration-dependent increase in (a) eGFP silencing (**Figure 2B**), (b) total lysosomal volume (**Figure 2C, Figure S2D**) and (c) cellular granularity (**Figure 2D, Figure S2C**) compared to untreated and siNG-transfected cells. In contrast, exposure of the cells to 20 µM doxazosin or terazosin could not phenocopy these effects, despite only minor structural differences relative to prazosin (**Figure 2A-D**). Of note, the relative mean fluorescence intensity (rMFI) in the siCTRL sample increased markedly upon treatment with 10-20 µM prazosin (**Figure S2A-B**), which is indicative of cell stress[66,67]. In addition to dextran NGs, a series of other siRNA nanocarriers was screened. Similar results were obtained for prazosin in combination with the commercially available polymeric transfection reagent *in vivo*-jetPEI® when used in serum-containing (10% FBS) cell medium (**Figure S3A-E**). In contrast, even 40 µM desloratadine did not have a substantial adjuvant effect on these NPs with only moderate improvement in knockdown observed at 250 nM siRNA, **Figure S3A**), despite clear indication that the applied desloratadine evoked the anticipated lysosomal swelling in all conditions tested (**Figure S3B**). Likewise, prazosin outperformed desloratadine in boosting the siRNA delivery of PEGylated DOTAP-DOPE liposomes (**Figure S4A, Figure S4C**) and only prazosin was able to moderately improve eGFP knockdown obtained with state-of-the-art LNPs containing the ionizable lipid DLin-MC3-DMA (MC3 LNPs, **Figure S4B, Figure S4D**). Earlier work by our group has demonstrated that CADs are mainly compatible with nanocarriers that promote the early release of siRNA in the endolysosomal compartment, with subsequent diffusion of the decomplexed siRNA through the CAD-induced pores in the limiting endolysosomal membrane[25]. In line with CADs, the cytosolic delivery efficiency of the siNGs can be markedly enhanced by prazosin, most likely linked to the straightforward release of the siRNA from the hydrogel network. Moreover, the adjuvant effect of PRA is much more outspoken when combined with PEGylated cationic liposomes in contrast to ionizable LNPs. It is known that the former nanocarriers relatively easily undergo decomplexation, while the latter retain their RNA payload stably complexed in the core of the particle.[25] As such, also for prazosin these data seem to corroborate the above-mentioned hypothesis of intra-endosomal carrier siRNA decomplexation followed by pore-induced cytosolic diffusion. Nevertheless, additional experiments would be required to validate this hypothesis. Altogether, from these data it is clear that prazosin has more outspoken effects on lysosomal swelling and siRNA delivery than desloratadine. However, prazosin also has a greater impact on cell viability (**Figure 2E**).

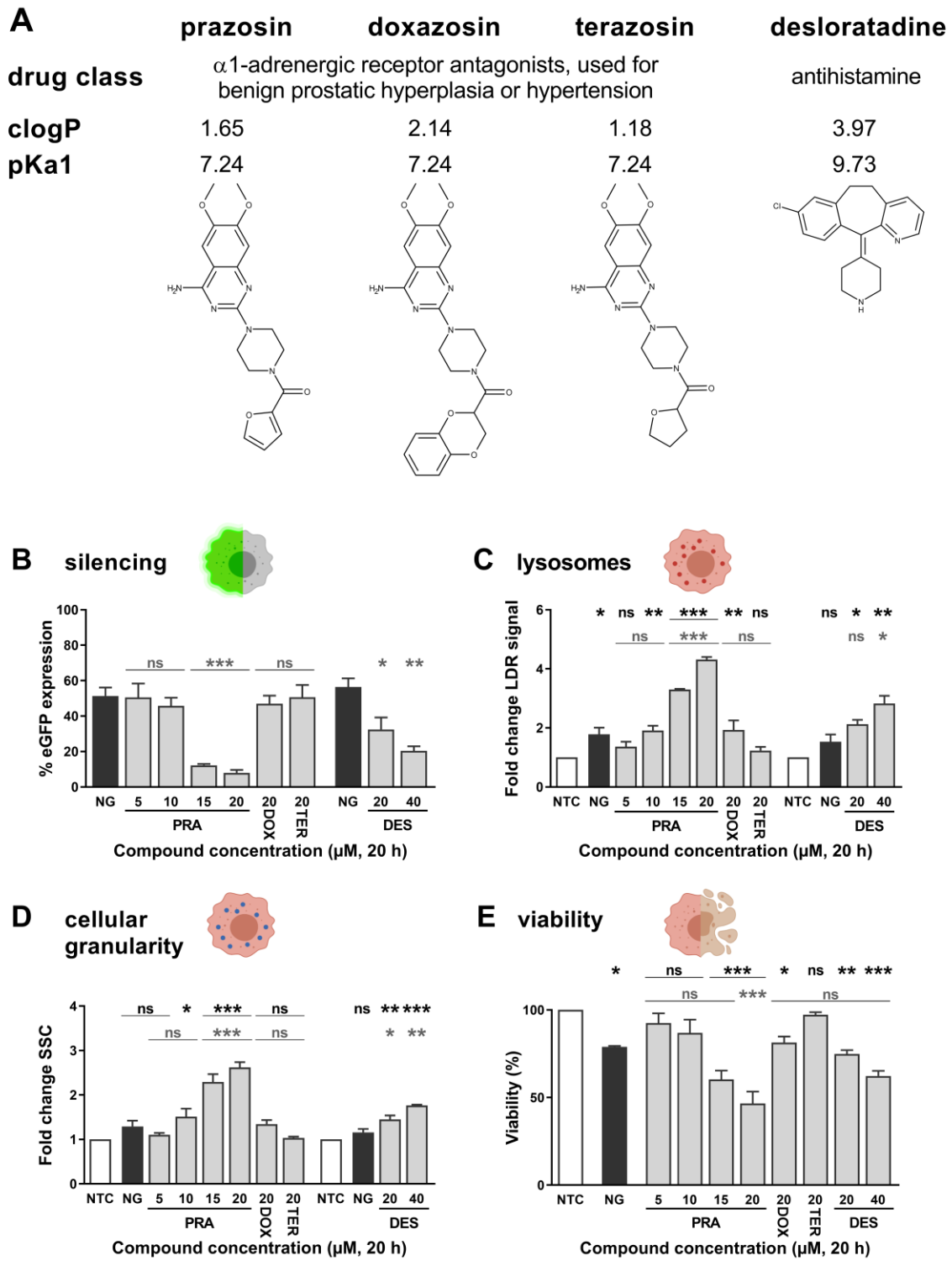

Figure 2. Prazosin and desloratadine, but not doxazosin or terazosin, improve the eGFP silencing potential of dex-HEMA siNGs in NSCLC cells, while increasing the lysosomal volume and cellular granularity. (A) The drug class, clogP, pKa1 values and molecular structure of prazosin (PRA), doxazosin (DOX), terazosin (TER) and desloratadine (DES). The pKa1 and clogP values of the compounds were predicted with JChem for Office (version 17.21.0.1797, ChemAxon Ltd., Budapest, Hungary)[68]. **(B)** Sequential treatment of siNG-transfected H1299-eGFP cells (1 nM siRNA) with the quinazolinamine-based 'non-CAD hit' PRA or the CAD DES caused significant additional eGFP silencing in a concentration-

dependent manner, while the quinazolinamines DOX and TER had no effect at 20 µM. **(C-D)** Fold change in Lysotracker™ Deep Red (LDR) signal and side scatter (SSC) signal, measured *via* flow cytometry, for H1299-eGFP cells sequentially transfected with dex-HEMA siNGs and treated with different concentrations of PRA/DOX/TER/DES for 20 h. **(E)** Cell viability of H1299-eGFP cells following sequential dex-HEMA siNG transfection and PRA/DOX/TER/DES addition for 20 h. Data are represented as mean ± the standard error of the mean (SEM) for three independent repeats. Statistical significance is indicated when appropriate, in black * when referring to the untreated control and in grey * when compared to dex-HEMA siNG transfection alone (ns $p > 0.05$, * $p \leq 0.05$, ** $p \leq 0.01$, *** $p \leq 0.001$). (clogP = calculated logP, pKa1 = pKa of the most basic amine, eGFP = enhanced green fluorescent protein, NG = dex-HEMA siNG transfection without sequential compound treatment, NTC = not treated control, ns = not significant).

Next, we used confocal fluorescence microscopy to visualize and quantify cytosolic delivery of Alexa Fluor® 647-labeled oligonucleotides (AF647 ONs), which upon endosomal escape migrate to the cell nucleus[25,69,70]. Hence, quantification of the AF647 ON fluorescence in the nuclear region of each individual cell can be used as a measure of endosomal escape efficiency. A punctate pattern was observed for most untreated cells and cells exposed to 20 µM doxazosin or terazosin (< 5% of labeled nuclei), indicating lysosomal sequestration of AF647 ON-loaded dextran NGs. In contrast, incubation with 15 or 20 µM prazosin and 40 µM desloratadine increased the amount of stained nuclei up to ~52-72% and ~31%, respectively (**Figure 3A, Figure S5A, Figure S6A-I**). Additionally, prazosin induced the formation of intracellular galectin-3 foci in H1299 cells expressing mCherry-galectin-3, while such foci were scarce in untreated cells. Galectin-3 is a cytosolic protein that acts as a membrane damage sensor, since it is able to bind carbohydrates on the luminal side of endolysosomes, which are exposed upon membrane damage[46,71]. These data indicate that the enhanced cytosolic delivery upon prazosin treatment is likely the result of an increased endolysosomal membrane permeability (**Figure S5B**).

Interestingly, in contrast to desloratadine, prazosin treatment also led to the rapid (< 1 h, data not shown) formation of large vacuoles (indicated with red arrows in **Figure 3** and **Figure S5A,C**), which has been reported previously for this compound[36,37]. Notably, both LysoTracker™ Deep Red positive (indicated with white circles in **Figure S2D**) and negative vacuoles (indicated with yellow circles in **Figure S2D**) could be observed, which corroborates earlier findings and indicates that not all vacuoles are acidic[37]. In addition, staining of compound-treated cells with the PLD detection reagent LipidTOX™ Red (**Figure 3B**, **Figure S5C, Figure S6J**) revealed that 40 µM desloratadine treatment, in line with our previously obtained

data[25,27], induced the accumulation of phospholipids in vesicular structures, while none of the applied prazosin concentrations could replicate this. Hence, these data altogether indicate that prazosin treatment results in a different cellular phenotype compared to the previously identified CAD adjuvants[25,27].

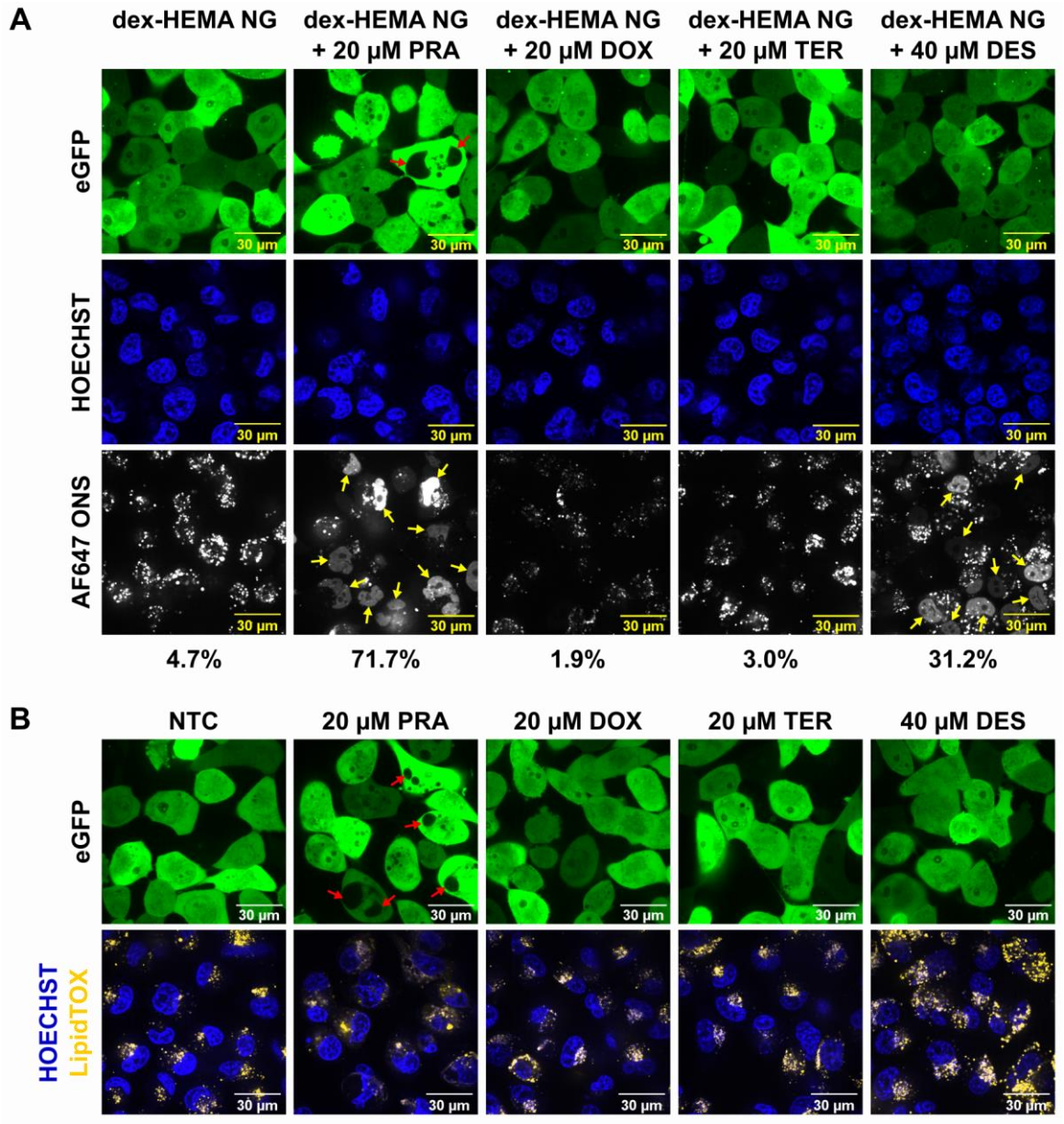

Figure 3. Both desloratadine and prazosin, but not doxazosin or terazosin, promote oligonucleotide release into the cytosol, while only desloratadine induces a phospholipidosis phenotype in NSCLC cells. (A) Representative confocal images from the intracellular AF647 oligonucleotide (ON) distribution in H1299-eGFP cells, only transfected with AF647 ON-loaded dex-HEMA NGs, or transfected cells subsequently incubated with 20 µM prazosin (PRA)/20 µM doxazosin (DOX)/20 µM terazosin (TER)/40 µM desloratadine (DES) for 20 h. Nuclei can be seen in blue, while cells in which endolysosomal escape happened show nuclear fluorescence in the red channel (red fluorescence is depicted white). The values below the images correspond to the percentage of cells with white nuclei (yellow arrows). The red arrows highlight the presence of vacuoles. **(B)** Representative confocal images

from the phospholipid distribution in H1299-eGFP cells visualized with LipidTOX™ Red PLD detection reagent in 20 µM PRA/20 µM DOX/20 µM TER/40 µM DES treated cells (20 h). The scale bar corresponds to 30 µm. (eGFP = enhanced green fluorescent protein, NTC = not treated control, NG = nanogels, AF647 = Alexa Fluor® 647 dye, NSCLC = non-small cell lung cancer).

In summary, the adjuvant effect of the 'non-CAD hit' prazosin and the inactive structural analogue terazosin could be confirmed, albeit prazosin clearly induced cell toxicity. However, we could not confirm the enhanced siRNA delivery of doxazosin, a minor hit in the primary screen at 20 µM, although an effect at higher concentrations cannot be ruled out. Most likely prazosin exerts its adjuvant effect *via* an off-target perturbation independently of its pharmacological action at the documented clinical target (α1-adrenergic receptor)[72]. First, micromolar prazosin concentrations are needed to be effective as a delivery-promoting compound[46] or cell death inducer[36–45], while nanomolar concentrations are sufficient to block the adrenergic receptor[37]. Second, the structurally very similar quinazolinamines terazosin and doxazosin (**Figure 2A**) did not have such an adjuvant effect, although they antagonize the same receptor. It is anticipated that the adjuvant effect of prazosin on siRNA delivery could be the result of its lysosomal accumulation. Despite a relatively low clogP value (**Figure 2A**), the presence of a protonatable amine group can still result in some degree of lysosomotropic behaviour. Indeed, studies have shown that a fluorescent derivative of prazosin co-localizes with the lysosomal compartment[36,37,46]. On the other hand, prazosin has also been shown to enter cells via a non-adrenoreceptor mediated endocytic uptake mechanism called transport-P, leading to its lysosomal sequestration[36]. Interestingly, comparison with a library of closely related structural analogues (including terazosin) revealed that the activation of the transport-P pathway seemed to be very specific for prazosin[73]. Notably, the described lysosomal localization of prazosin and the lysosomal accumulation of siNGs demonstrated in earlier work[14,74], suggests that the majority of siRNAs are released from the lysosomal compartment. A recent report similarly identified prazosin as a compound that can boost the transport of soluble and cell-associated antigens from endolysosomal compartments into the cytosol and subsequently enhance cross-presentation in dendritic cells[46]. Nevertheless, to the best of our knowledge, the presented study is the first to show that prazosin can boost siRNA delivery in cancer cells by increasing endolysosomal escape. Notably, also other studies revealed damaging effects of prazosin on the endolysosomal system in a similar concentration range, *e.g.* inhibition of endocytic sorting[75] and tubulation

of endosomes/lysosomes[36,37,75,76], which subsequently led to inhibition of cytokinesis[37,38,75]. Prazosin induced a remarkably different phenotype (*i.e.* vacuolization, absence of PLD, higher cytotoxicity) compared to our typical lysosomotropic CAD adjuvant desloratadine. Hence, in conjunction with the absence of a similar lysosomal phenotype for the physicochemically equivalent terazosin and doxazosin, these data suggest that the siRNA delivery-promoting effect of prazosin is not solely linked to lysosomal accumulation and PLD induction as proposed for CAD molecules[49]. Interestingly, similar differences in other cellular activities (*e.g.*, cell death induction[42,43,77], inhibition of endocytic sorting[75] or increase in dendritic cell cross-presentation[46]) of the three tested quinazolinamines have been reported in the literature, with terazosin and prazosin being inactive or most effective, respectively.

PIKfyve inhibitors induce pronounced vacuolization with limited adjuvant effect

Our data clearly indicate that prazosin induces a distinct cellular phenotype than typical CAD adjuvants[22,25,27,33]. Indeed, prazosin-treated cells are, in contrast to desloratadine-treated cells, characterized by large cytoplasmic vacuoles, while PLD induction was not observed. Consequently, these findings prompted us to investigate if other physicochemical, structural and pharmacological non-related (drug) compounds that are known to induce marked vacuolization can also have an adjuvant effect on siRNA delivery. Hence, we evaluated if post-incubation (20 h) with four well-known phosphatidyl 3-phosphate 5-kinase (PIKfyve) inhibitors (apilimod[78,79], vacuolin-1[80], YM-201636[79,81] and APY-0201[79,82]) (**Figure 4A**) could improve the gene-silencing potential of dex-HEMA siNGs in NSCLC cells. Although these compounds show high lipophilicity (clogP > 3), which allows them to easily diffuse across cell membranes, they are not anticipated to act as typical CADs as the pKa of the basic amine is too low (pKa1 < 6).

Albeit lower concentrations of these compounds (nM range) have previously shown to induce vacuolization in other cell types[81,83–87], the appearance of large translucent cytoplasmic vacuoles in H1299-eGFP cells (**Figure S7**) was only observed in the low micromolar range. While the tested compounds were overall well tolerated (except for 10 µM APY-0201, **Figure 4E**), all PIKfyve inhibitors induced an increase in (a) eGFP silencing (**Figure 4B**), (b) lysosomal volume (**Figure 4C**) and (c) cellular granularity (**Figure 4D**) compared to untreated and siNG-transfected cells. The formation of cytoplasmic vacuoles (as can be seen in the eGFP channel) and the marked enlargement of Lysotracker™ Deep Red -labeled vesicles upon

PIKfyve inhibitor treatment were also visually confirmed with confocal microscopy (**Figure 5A**). Note that the majority of the large vacuoles were Lysotracker™ positive, suggesting that these large, swollen vesicles are of late endosomal or lysosomal origin in our cell model. In addition, staining of the PIKfyve inhibitor-treated cells with the PLD detection reagent LipidTOX™ Red (**Figure 5B**, **Figure S8**), revealed that there was also an accumulation of phospholipids in these vacuoles, albeit not to the same extent for all compounds. This PLD phenotype is clearly different from desloratadine treatment, where phospholipids seem to accumulate in much smaller vesicular structures (**Figure 5B**). Interestingly, the PIKfyve inhibitor that induced the most apparent lysosomal swelling (**Figure 4C**) and vacuolization (**Figure S7**), but the least PLD induction (**Figure 5B**, **Figure S8**) (*i.e.* APY-0201) also had the greatest effect on eGFP silencing. However, as PIKfyve inhibition has also shown to inhibit autophagy[80,87–89], exocytosis[90], endosomal maturation[91] and endosome-to-trans-Golgi network retrograde transport[92], it cannot be excluded that these effects might likewise play a role[22]. Of note, despite the extensive vacuolization in these cells, the eGFP knockdown enhancement was inferior to that observed following prazosin treatment, suggesting that also for prazosin other cellular mechanisms than mere vacuolization are involved in improved siRNA delivery.

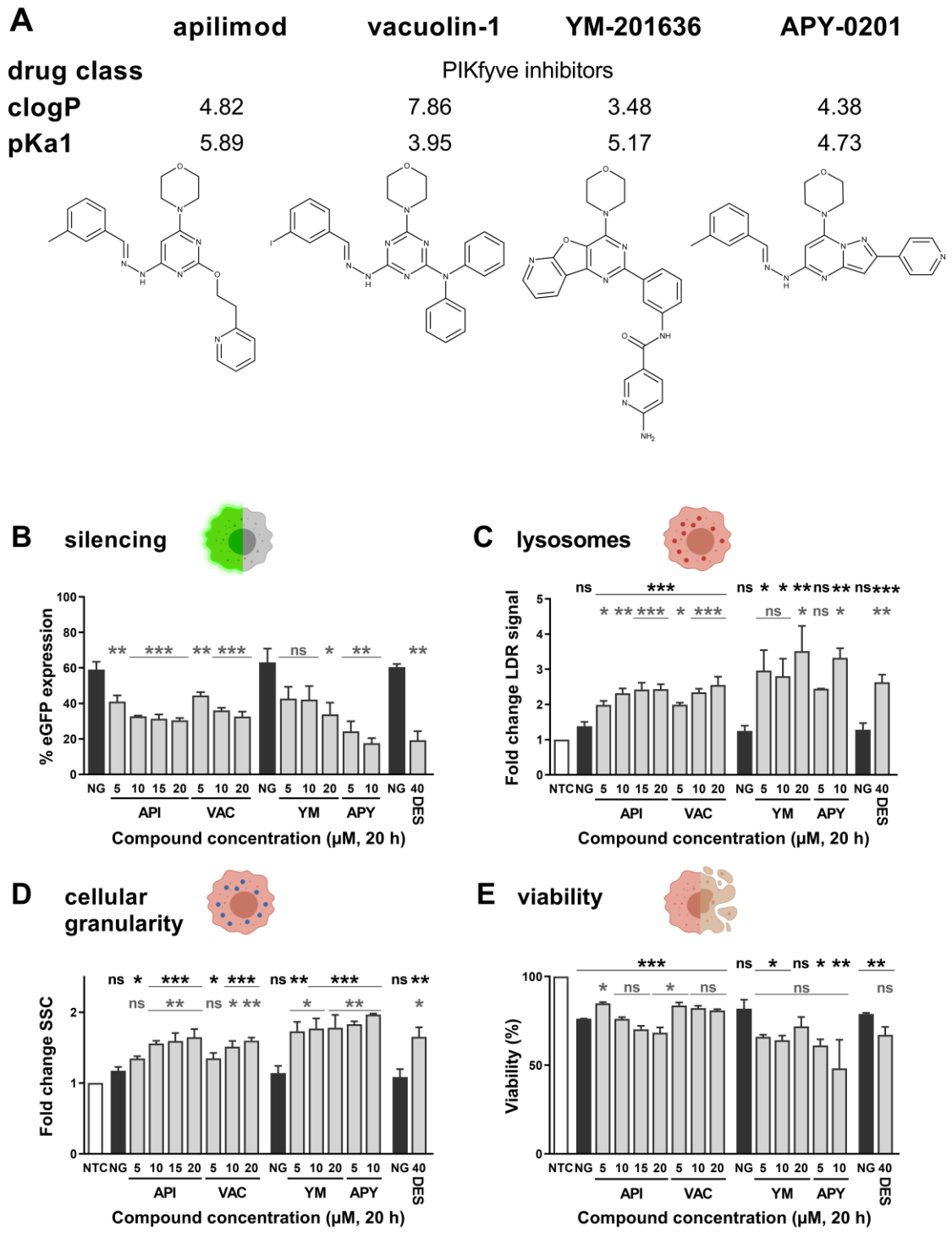

Figure 4. PIKfyve inhibitors improve the eGFP silencing potential of dex-HEMA siNGs in NSCLC cells to a limited extent, while increasing the lysosomal volume and cellular granularity. (A) The drug class, clogP, pKa1 values and molecular structure of apilimod (API), vacuolin-1 (VAC), YM-201636 (YM) and APY-0201 (APY)[68]. The pKa1 and clogP values of the compounds were predicted with JChem for Office (version 17.21.0.1797, ChemAxon Ltd., Budapest, Hungary)[68]. **(B)** Sequential treatment of siNG-transfected H1299-eGFP cells (1 nM siRNA) with PIKfyve inhibitors caused significant additional eGFP silencing, albeit the effect was generally lower than the CAD desloratadine (DES). **(C-D)** Fold change in Lysotracker™ Deep Red (LDR) signal and side scatter (SSC) signal, measured *via* flow

cytometry, for H1299-eGFP cells sequentially transfected with dex-HEMA siNGs and treated with different µM concentrations of API/VAC/YM/APY/DES for 20 h. **(E)** Cell viability of H1299-eGFP cells following sequential dex-HEMA siNG transfection and API/VAC/YM/APY/DES addition for 20 h. Data are represented as mean ± the standard error of the mean (SEM) for three independent repeats (except viability, which is done in two independent repeats). Statistical significance is indicated when appropriate, in black * when referring to the untreated control and in grey * when compared to dex-HEMA siNG transfection alone (ns $p > 0.05$, * $p \leq 0.05$, ** $p \leq 0.01$, *** $p \leq 0.001$). (clogP = calculated logP, pKa1 = pKa of the most basic amine, eGFP = enhanced green fluorescent protein, NG = dex-HEMA siNG transfection without sequential compound treatment, NTC = not treated control, ns = not significant).

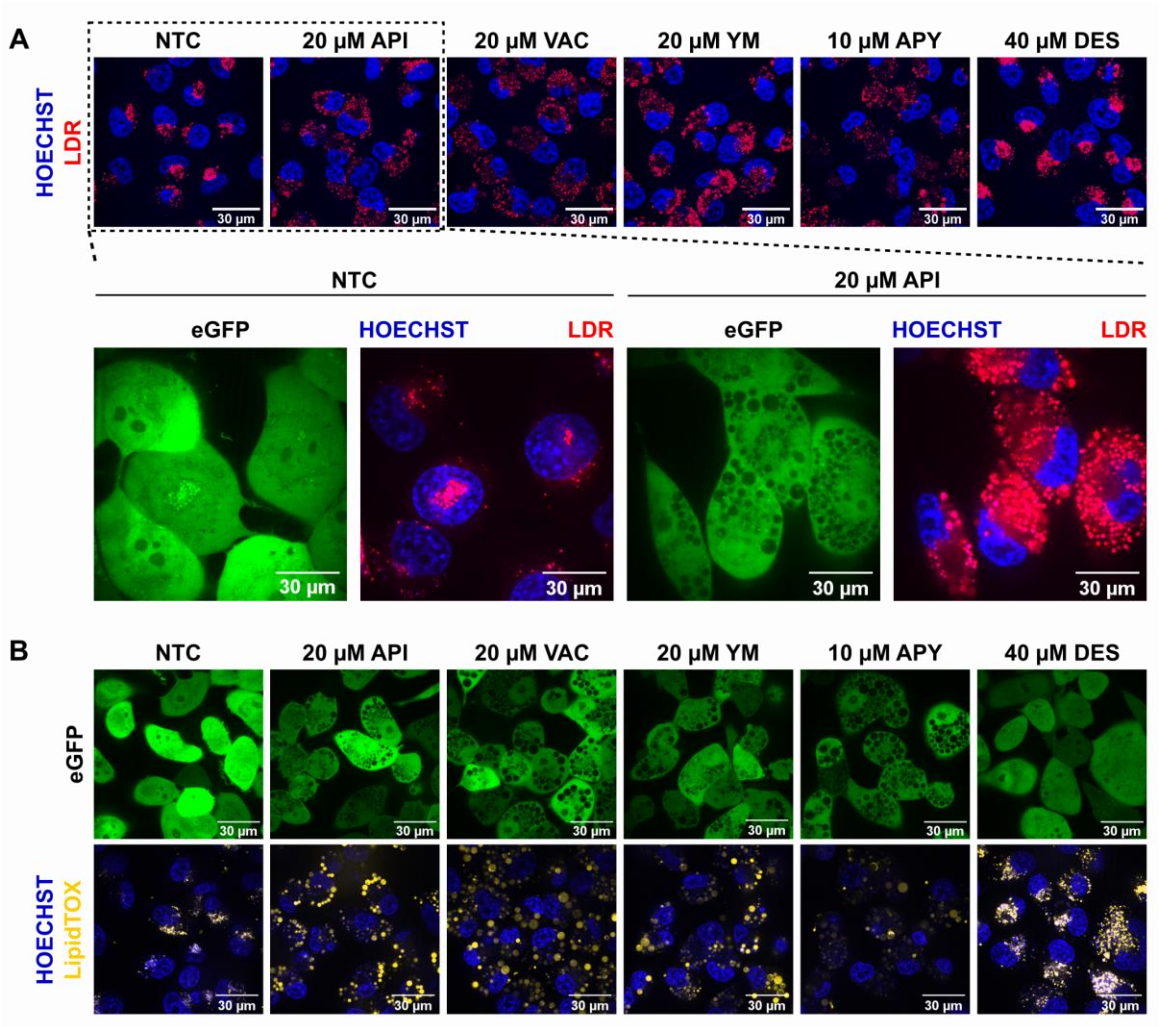

Figure 5. Several PIKfyve inhibitors and desloratadine induce varying degrees of lysosomal swelling and phospholipidosis in NSCLC cells. (A) Representative confocal images showing the lysosomal compartment (red) following LysoTracker™ Deep Red (LDR) labeling for untreated and 20 µM apilimod (API)/20 µM vacuolin-1 (VAC)/20 µM YM-201636 (YM)/10 µM APY0201 (APY)/40 µM desloratadine (DES) treated H1299-eGFP cells (20 h). **(B)** Representative confocal images from the phospholipid distribution in H1299-eGFP cells visualized with LipidTOX™ Red PLD detection reagent in 20 µM API/20 µM VAC/20 µM YM/10 µM APY/40 µM DES treated cells (20 h). The scale bar corresponds to 30 µm. (eGFP = enhanced green fluorescent protein, NTC = not treated control).

Prazosin improves silencing of cholesterol-siRNA conjugates

Covalent conjugation of (targeting) ligands to the siRNA strands can be an effective and simple alternative to NP-based delivery. While N-acetylgalactosamine (GalNAc)-siRNA conjugates, which target the asialoglycoprotein receptor on hepatocytes, are now clinically validated drugs[10], their use is largely restricted to liver-related diseases. Hence, other self-deliverable siRNAs that are able to reach tissues or tumors are highly sought after[71,93]. In this context, siRNAs modified with lipids such as cholesterol-linked siRNAs (chol-siRNAs) are one of the most reported conjugates[93–99] that have shown *in vivo* accumulation and gene silencing in solid tumors[99–101]. However, despite adequate accumulation and endocytic internalization, high conjugate concentrations are still needed, both *in vitro* and *in vivo*, to achieve significant knockdown due to inefficient endosomal escape[3,13,20,71]. Hence, we evaluated here if prazosin and desloratadine could similarly improve the cytosolic delivery of two cholesterol-conjugated eGFP-targeting siRNAs with different sequences in H1299-eGFP cancer cells. As shown in **Figure 6A** and **Figure S9A**, the intrinsic silencing potential of both chol-siRNAs was low, with chol-siRNA 1 inducing less than 10% eGFP silencing at 250 nM, while chol-siRNA 2 was slightly more potent (~30% eGFP silencing at 250 nM). Whereas sequential treatment for 20 h with 40 µM desloratadine had little impact on the silencing efficiency, the application of 20 µM prazosin achieved up to 90% eGFP knockdown, despite clear indication that both compounds evoked lysosomal swelling (**Figure 6B-C** and **Figure S9B-C**). Notably, 20 µM prazosin induced a significant drop in cell viability (**Figure 6D**), in line with the aforementioned data on dex-HEMA siNGs (**Figure 2E**). Other CADs (*e.g.* amitriptyline, siramesine, loperamide and chloroquine) have recently shown to facilitate endosomal escape of chol-siRNAs in other cancer cells (*e.g.*, HeLa)[71]. Here it was demonstrated that the fraction of damaged endocytic vesicles that also contain chol-siRNA was highly dependent on the type of CAD, leading to differences in target gene knockdown[71]. Hence, this might in part explain the absence of an adjuvant effect for desloratadine in our experiments. In summary, next to polymeric NPs, we could confirm the significantly larger adjuvant effect of prazosin, compared to desloratadine, on gene knockdown *via* chol-siRNAs.

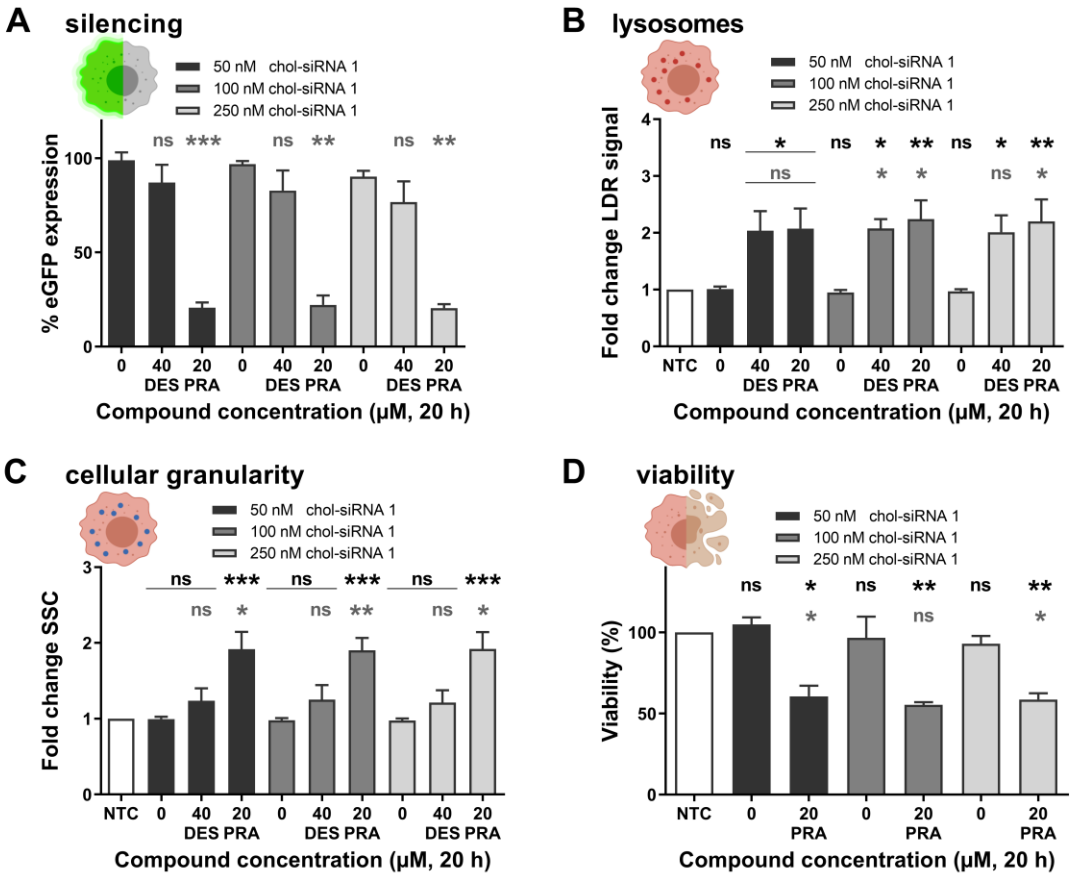

Figure 6. Prazosin, but not desloratadine, enhances eGFP silencing potential of chol-siRNAs in NSCLC cells. (A) Sequential treatment of chol-siRNAs (different concentrations) with 20 μM prazosin (PRA) caused a significant additional eGFP silencing, while 40 μM desloratadine (DES) had no effect. **(B-C)** Fold change in LysoTracker™ Deep Red (LDR) and side scatter (SSC) signal, measured *via* flow cytometry, for H1299-eGFP cells sequentially transfected with chol-siRNAs and treated with 40 μM DES or 20 μM PRA for 20 h. **(D)** Cell viability of H1299-eGFP cells following sequential chol-siRNA transfection and 20 μM PRA addition. Data are represented as mean ± the standard error of the mean (SEM) for two independent repeats. Statistical significance is indicated when appropriate, in black * when referring to the untreated control and in grey * when compared to chol-siRNA transfection alone (ns $p > 0.05$, * $p \leq 0.05$, ** $p \leq 0.01$, *** $p \leq 0.001$). (eGFP = enhanced green fluorescent protein, NTC = not treated control, ns = not significant, chol-siRNA = cholesterol-conjugated siRNA, NSCLC = non-small cell lung cancer).

Towards prazosin drug combination therapy in oncology

Given that prazosin can boost the cytosolic delivery of siRNA, while also having a direct pro-apoptotic activity (as suggested by our experimental data and as shown by others[36–42,45]), the combination of prazosin and siRNA can open up avenues for synergistic anti-cancer therapy. Indeed, siRNAs are often studied to enhance the tumor killing efficacy of low molecular weight anti-cancer drugs *e.g. via* silencing of efflux multidrug resistance proteins

(*e.g.* multidrug resistance protein 1 (MDR-1)[102–104]) to increase the drug concentration in the target cells. In this work, as prazosin strongly improves siRNA delivery, a synergistic tumor killing effect could be envisioned when selecting a siRNA that triggers a complementary cell death pathway (**Scheme 1**). Importantly, it can be rationalized from the literature that prazosin holds the potential to enhance siRNA delivery to (cancer) cells *in vivo*. Indeed, systemic administration of non-toxic prazosin concentrations could specifically reduce xenograft tumor growth (and/or mice survival) *via* a direct anti-proliferative effect[42] or by enhancing cross-presentation[46], both independently of its anti-adrenergic activity. Cancer selectivity is an important trait for anticancer drugs. Of note, while CADs have been described to induce cancer cell-specific lysosomal cell death due to the altered sphingolipid metabolism in transformed cells[34], the dose-dependent cytotoxicity of prazosin to cancer cells as compared to healthy cells still merits further investigation. In addition, local administration (*e.g.,* intratumoral injection) of the prazosin adjuvant in combination with chol-siRNAs might be a valuable option to induce synergistic tumor cell killing, while avoiding systemic exposure to high drug concentrations. For example, modified chol-siRNAs have shown to widely distribute throughout xenografted glioblastoma tumors upon intratumoral injection and subsequently produce functional knockdown[105]. We anticipate that our results could be extrapolated to other lipid-modified siRNAs as well, which recently have shown gene silencing potential in extrahepatic tissues[98]. Furthermore, co-encapsulation of prazosin and siRNA in a lipid- or polymer-based nanocarrier could allow spatiotemporally controlled delivery of both drugs at the cellular level[24], which could enable other administration routes and facilitate *in vivo* translation. In this regard, our group recently reported on the integration of tricyclic CADs in lipid-like nanoparticles for improved delivery of RNA therapeutics[23]. It would be of interest to investigate if this approach could likewise be applied on less hydrophobic quinazolinamine derivatives such as prazosin.

The documented *in vitro* and *in vivo* anti-tumor activity of quinazolines includes, besides apoptosis induction[36–44], the activation of the metastasis-protective anoikis effect[106], the inhibition of tumor-angiogenesis[107] and the abovementioned enhancement of cross-presentation in dendritic cells by prazosin, both *in vitro* and *in vivo* [46]. The process of cross-presentation (**Scheme 1**) involves the internalization of exogenous proteins (*e.g.,* cell-associated antigens released by dying cancer cells) by antigen-presenting cells, which are subsequently broken down into short peptides that can be loaded onto Major

Histocompatibility Complex class I (MHC I) molecules. In this way, tumor antigens are presented to naive antigen-specific $CD8^+$ T-cells, which require this activation step to proliferate and differentiate into effector cytotoxic T lymphocytes[46,108]. Two main cross-presentation pathways have been described. In the vacuolar pathway, antigens are processed by endolysosomal proteases and directly loaded on MHC I molecules within the endocytic compartment. In contrast, the cytosolic pathway (**Scheme 1**) involves endosome-to-cytosol antigen import, where proteasomal degradation produces peptides that are delivered to the lumen of MHC I-containing compartments (*e.g.* endoplasmic reticulum, ER) *via* the transporter for antigen presentation (TAP)[46,108,109]. Interestingly, albeit the relative involvement of both models in *in vivo* cross-presentation remains unclear, the endolysosomal escape of antigens into the cytosol has shown to be a crucial and rate-limiting step in the cytosolic pathway[46,109]. Similar to our results with siRNA, prazosin has shown to enhance the efficiency of this TA endosome-to-cytosol transport in dendritic cells, leading to a synergistic effect with checkpoint anti-tumor immunotherapy in a melanoma xenograft mouse model[46]. As combination therapies are the mainstay of clinical cancer care, it has been previously postulated to increasingly allow nanomedicines to synergize with pharmacological and physical co-treatments[110]. This recently published study together with the data presented in this work suggest that a multifaceted anti-cancer combination strategy could potentially be pursued with prazosin.

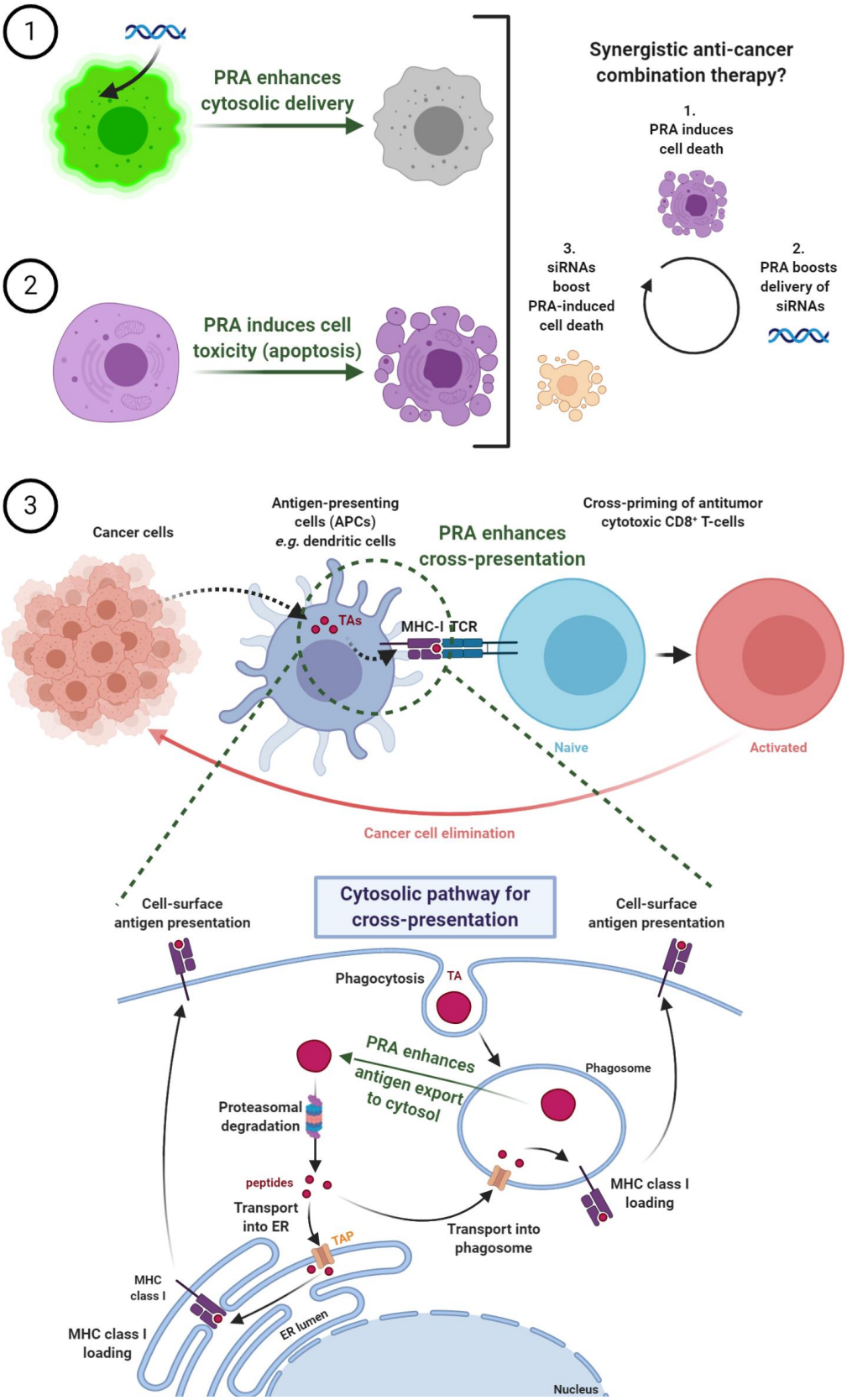

Scheme 1. Schematic illustration of the main anti-tumor actions of prazosin. (1-2) As prazosin (PRA) can boost the cytosolic delivery of siRNA, while also having a direct pro-apoptotic activity, the combination of PRA and a therapeutic siRNA (*e.g.* against efflux multidrug resistance proteins, anti-apoptotic proteins, *etc.*) can open up avenues for synergistic treatment in the context of anti-cancer

therapy. Ideally, PRA would improve the functional delivery of these siRNAs, which in turn may boost the PRA-induced cell death. **(3)** Interestingly, similar to the observed boost in endolysosomal escape of siRNA molecules, PRA has also been described as a molecule that can improve the import of tumor antigens (TAs) from the endolysosomes into the cytosol of dendritic cells, thus improving cross-presentation (*i.e.* presentation of TAs on Major Histocompatibility Complex class I molecules) and -priming, which is necessary for cytotoxic T lymphocyte-mediated anti-tumor immune responses. (MHC class I = Major Histocompatibility Complex class I molecules, TA = tumor antigen, ER = endoplasmic reticulum, TAP = transporter for antigen presentation, TCR = T-cell receptor). Figure created with BioRender.com.

3. CONCLUSION

Inefficient intracellular delivery remains one of the most important barriers for nucleic acid therapeutics. We recently discovered that multiple cationic amphiphilic drugs (CADs) can be repurposed as cytosolic delivery-promoting adjuvants of siRNA and antisense oligonucleotides in distinct cancer cell lines. In this work, we further demonstrated that other small molecular drugs, which do not have the typical physicochemical properties of CADs, can likewise be repurposed as siRNA delivery enhancers. Most importantly, our data indicate that prazosin, a quinazolinamine-based α1-adrenergic antagonist, can both induce cell death and increase the permeability of endolysosomes for small nucleic acid cargo. Consequently, we anticipate that the gained insights will fuel further experiments in which the prazosin adjuvant approach is used in a combination therapy that could potentially provide synergistic anti-cancer effects.

4. MATERIALS AND METHODS

siRNA duplexes and oligonucleotides

The 21mer siRNA duplexes targeted against the enhanced green fluorescent protein (eGFP, sieGFP) and the negative control siRNA (siCTRL) were purchased from Eurogentec (Seraing, Belgium). The 19mer cholesterol (chol)-conjugated siRNAs (Accell, chol-siRNA 2) were purchased from Dharmacon (Lafayette, CO, USA). The other chol-conjugated siRNAs (chol-siRNA 1) with siSTABLE modifications were also purchased from Dharmacon (Lafayette, CO, USA). Dicer substrate asymmetric 25/27mer siRNA duplexes targeting eGFP (DsieGFP) or *firefly* luciferase (DsiFLuc) were provided by Integrated DNA Technologies BVBA (IDT, Leuven, Belgium). The used negative controls consist of a sequence that has no relevant homology to any known eukaryotic gene sequences. Alexa Fluor® 647 labeled 21mer oligonucleotides (AF647 ONs) were from Eurogentec (Seraing, Belgium). The concentration of the siRNA/ON stock solutions in nuclease-free water (Ambion®-Life Technologies, Ghent, Belgium) was calculated from absorption measurements at 260 nm (1 OD260 = 40 μg mL^{-1}) with a NanoDrop 2000c UV-Vis spectrophotometer (Thermo Fisher Scientific, Rockford, USA). The sequences and modifications of the applied (chol-conjugated) siRNA duplexes/ONs are summarized in **Table S2**.

Nanoparticle synthesis, preparation and siRNA complexation

Using an inverse miniemulsion photopolymerization method as previously reported, dextran hydroxyethyl methacrylate (dex-HEMA, degree of substitution (DS) of 5.2) was copolymerized with a cationic methacrylate monomer [2-(methacryloyloxy)ethyl]-trimethyl-ammonium chloride (TMAEMA) to produce cationic dex-HEMA-*co*-TMAEMA nanogels (hereafter abbreviated as dex-HEMA NGs)[14,111–113]. The synthesized NGs were lyophilized and stored desiccated to ensure long-term stability. To produce siRNA-loaded NGs (siNGs) for *in vitro* experiments, a NG stock (2 mg/mL) was prepared by dispersing a weighed amount of NGs in ice-cooled nuclease-free water (Ambion®-Life Technologies, Ghent, Belgium), followed by brief sonication (3 x 5 sec, amplitude 10%; Branson Ultrasonics Digital Sonifier®, Danbury, USA). Next, equal volumes of NGs and siRNA in 4-(2-hydroxyethyl)-1-piperazineethanesulfonic acid (HEPES) buffer (20 mM, pH 7.4) were mixed and allowed to incubate on ice for 10 min, prior to further dilution in Opti-MEM® (Invitrogen, Merelbeke, Belgium). This complexation procedure was applied for all cell-based experiments in a 96-well

plate and resulted in a 30 µg/mL NG dispersion loaded with 1 nM siRNA (0.033 pmol siRNA/µg NGs or 0.1 pmol siRNA/well), unless indicated otherwise.

To obtain PEGylated cationic liposomes, (2,3-dioleoyloxy-propyl)-trimethylammonium (DOTAP), 1,2-dioleoyl-*sn*-glycero-3-phosphoethanolamine (DOPE) and 1,2-distearoyl-*sn*-glycero-3-phosphoethanolamine-N-[methoxy(polyethylene glycol)-2000] (DSPE-PEG_{2000}) were purchased from Avanti Polar Lipids, Inc. (Alabaster, AL, USA) as solutions in chloroform. PEGylated (corresponding to 5 mol% of the total lipids) DOTAP-DOPE (1:1 molar ratio) liposomes were prepared *via* the lipid film hydration method by mixing appropriate amounts of the mentioned lipids in a round bottom flask. Rotary evaporation under vacuum at 40 °C resulted in a lipid film, which was subsequently hydrated using 1 mL HEPES buffer (pH 7.4, 20 mM). The lipid dispersion was vortexed and sonicated using a probe sonicator (1 min, amplitude 10%; Branson Ultrasonics Digital Sonifier®, Danbury, USA) to obtain a monodisperse 2 mM liposome dispersion (total lipid concentration). Next, PEGylated DOTAP-DOPE liposomes were complexed with siRNA at an optimal charge ratio (nitrogen/phosphate ratio) equal to eight.[114] Hereto, equal volumes of liposomes and siRNA in HEPES buffer were mixed and allowed to complex at room temperature for 30 min prior to further dilution in Opti-MEM® and transfection. Preparation of DsiRNA-loaded ionizable lipid (MC3)-based lipid nanoparticles (MC3 LNPs) and siRNA-*in vivo*-jetPEI® polyplexes is described in supplementary information.

Cell lines and cell culture conditions

Cell culture experiments were performed using a human non-small cell lung epithelial carcinoma cell line (H1299) stably expressing eGFP (H1299-eGFP) or the wild type variant (H1299-WT, ATCC® CRL-5803™), respectively obtained from the lab of Prof. Camilla Foged (Department of Pharmacy, University of Copenhagen, Denmark) and the American Type Culture Collection (ATCC, Manassas, USA)[25,27,115,116]. H1299 cells (H1299-WT and H1299-eGFP) were cultured in Roswell Park Memorial Institute (RPMI) 1640 culture medium, supplemented with 10% fetal bovine serum (FBS, Hyclone™, GE Healthcare, Machelen, Belgium), 2 mM L-Glutamine and 100 U/mL penicillin/streptomycin (hereafter collectively called 'complete cell culture medium' or CCM). Cells were cultured at 37 °C in a humidified atmosphere containing 5% CO_2 and were passed every 3 days using a 0.25% trypsin-ethylenediaminetetraacetic acid (EDTA) solution to maintain subconfluency. H1299-eGFP cells were treated with CCM containing 1 mg/mL Geneticin® once per month to allow eGFP

transgene selection. All cells were regularly tested and found negative for mycoplasma. All cell culture products were purchased from Gibco®-Life Technologies (Grand Island, NY, USA) unless specifically mentioned otherwise.

Quantification of transfection efficiency and lysosomal volume of nanoparticle transfection and sequential adjuvant treatment by flow cytometry

To quantify gene silencing efficiency and lysosomal volume, H1299-eGFP cells were seeded in 96-well plates (VWR, Radnor, USA) at a density of 7500 cells/well (100 µL/well) and were allowed to settle overnight. Next, the cells were transfected with dex-HEMA siNGs (0.1 pmol siRNA/well, prepared as described above) or PEGylated DOTAP-DOPE siRNA-loaded liposomes (50 nM siRNA, prepared as discussed above) during 4 h at 37 °C in a humidified atmosphere containing 5% CO_2. For chol-siRNA experiments, cells were transfected for 6 h in Opti-MEM® as previously described[71]. Note that for every sieGFP condition a siCTRL sample was included to account for potential off-target effects. Subsequently, the transfection dispersion was removed and the cells were washed with phosphate buffered saline ($PBS^{-/-}$, no calcium, no magnesium) and subsequently received 50 µL fresh (DMSO control) or compound-containing CCM at the indicated concentrations (maximally 0.08% (v/v) residual DMSO). Note that apart from the NIHCC-compounds (described in our previous work[25]), all small molecules were obtained from Cayman Chemicals (Michigan, USA), except terazosin HCl dihydrate and YM-201636 which were from LKT Laboratories Inc. (St. Paul, USA) and Invivogen (San Diego, CA), respectively. Stock solutions were prepared in sterile-filtered BioPerformance Certified dimethyl sulfoxide (DMSO, Sigma-Aldrich, Overijse, Belgium). After 20 h, the small molecule containing CCM (and DMSO control) was removed and cells were kept in 50 µL fresh CCM for an additional 24 h. Following labeling of lysosomes with the LysoTracker™ Deep Red (LDR) probe (Molecular Probes™, Eugene, OR, USA) through incubation with 50 µL 75 nM LDR in CCM for 30 min at 37 °C, flow cytometry analysis was performed. Sample preparation consisted of detachment with 30 µL 0.25% trypsin-EDTA, neutralization with 120 µL CCM and a transfer of the cell suspensions to an U-bottom 96-well plate (Greiner Bio-One GmbH, Vilvoorde, Belgium), which was centrifuged during 5 min at 500 g. After removal of 120 µL supernatant, the cells were resuspended in 80 µL flow buffer ($PBS^{-/-}$ with 1% (v/v) FBS (Hyclone™, GE Healthcare, Machelen, Belgium) and 0.1% (w/v) sodium azide (Sigma Aldrich, Overijse, Belgium)) and kept on ice until analysis. For each sample the forward and side scatter (respectively FSC and SSC) as well as the green and red fluorescent signal of single cells were

measured. The samples were excited with the 488 and 638 nm laser lines and the signal was detected with the 525/40 and 660/20 filters using the CytoFLEX flow cytometer with plate loader for 96-well plates (Beckman Coulter, Krefeld, Germany) and CytExpert software. FlowJo software (Tree Star Inc., Ashland, OR, USA) was used for data analysis. The calculated percentages eGFP expression (*i.e.* the eGFP expression of cells treated with sieGFP was normalized to the expression of cells treated with a siCTRL under the same conditions) and fold changes in LDR signal intensity/SSC signal are presented as the mean ± standard error of the mean (SEM) for minimum 3 independent repeats (biological replicates), unless otherwise indicated.

In an additional experiment (**Figure S7A-B**), H1299-eGFP cells (seeded at 35000 cells/well) were transfected in 24-well plates with dex-HEMA siNGs for 4 h at 37 °C and subsequently treated with compounds as described before[27]. Transfection procedure and transfection efficiency determination for *in vivo*-jetPEI® and MC3 LNPs is described in supporting information.

Cell viability

H1299-eGFP cells were seeded, transfected with dex-HEMA siNGs/chol-siRNAs and treated with the compounds similar to the silencing experiments. The cell viability was determined with the CellTiter GLO® assay (Promega, Belgium), according to the manufacturer guidelines. Before initiating the assay, the culture plates and reconstituted assay buffer were placed at room temperature for 30 min. Next, the CCM was replaced by 100 µL fresh CCM and an equal volume of assay buffer was added. To induce complete cell lysis, the plates were shaken during 2 min and the signal was allowed to stabilize the following 10 min. Next, 100 µL from each well was transferred to an opaque 96-well plate, which was measured with a GloMax® 96 Microplate Luminometer (Promega, Belgium). Data are presented as the mean cell viability (%, percentage of luminescent signal relative to non-treated cells (NTC) for each condition) ± standard error of the mean (SEM) for three independent repeats (or a biological duplicate in **Figure 4E** and **Figure 6D**).

Visualization and quantification of the cytosolic release of AF647 ONs

H1299-eGFP cells were seeded at 75000 cells/compartment in 35mm diameter glass bottom microscopy dishes with 4 compartments (Greiner Bio-One GmbH, Germany) and were allowed to settle overnight. After removal of the complete cell culture medium (CCM), the cells were transfected with 300 µL of a 30 µg/mL NG dispersion loaded with 50 nM AF647 ONs

(= 1.667 pmol AF647 ONs/µg NGs). Following incubation for 4 h (37 °C, 5% CO_2), the ON-NG dispersion was removed and the cells were washed once with dextran sulfate sodium salt (Sigma-Aldrich, Overijse, Belgium, 1 mg/mL in PBS) and once with phosphate buffered saline (PBS, Invitrogen, Merelbeke, Belgium). Next, the cells received 500 µL fresh CCM, containing different µM concentrations of small molecular compounds or a DMSO control, for 20 h (37 °C, 5% CO_2). After removal of the small molecule-containing CCM, the nuclei were labeled with Hoechst 33342 (Molecular Probes™, Belgium) in CCM (1 mg/mL in water, 1/1000 dilution) during 15 min at 37 °C. Finally, the Hoechst solution was removed, fresh CCM was added and cells were kept at 37 °C in a humidified atmosphere containing 5% CO_2 until imaging. A spinning disk confocal (SDC) microscope (Nikon eclipse Ti, Japan), equipped with a MLC 400 B laser box (Agilent technologies, California, USA), a Yokogawa CSU-X confocal spinning disk device (Andor, Belfast, UK), an iXon ultra EMCCD camera (Andor Technology, Belfast, UK), a Plan Apo VC 60× 1.4 NA oil immersion objective lens (Nikon, Japan) and NIS Elements software (Nikon, Japan) was applied for imaging. The 408 nm, 488 nm and 663 nm laser lines were, respectively, used to excite the DAPI-labeled nuclei, the eGFP protein and the fluorescence resulting from AF647 ONs. A wait command of 0.2 seconds in between the image acquisition of the 3 channels was applied to avoid spectral overlap of the DAPI dye and the eGFP protein. If endolysosomal escape occurs, the labeled ONs will spread towards the cytosol, dequench and finally accumulate into the nucleus[25,69,70]. During data analysis with ImageJ (FIJI) software, both the total cell number and amount of cells with AF647 ON-positive nuclei were counted. Nuclei were detected in the blue channel by thresholding (applying the same offset values for every image) and intensity analysis (mean grey value), of the nuclear fluorescence signal in the red channel, was done. Using the 6th version of the GraphPad Prism software, these intensity values were plotted in frequency distributions and based on these histograms, a percentage of cells with AF647 ON-positive nuclei was determined. Data are represented as the percentage of cells with AF647 ON-positive nuclei for at least 496 cells in minimum 54 images.

Phospholipidosis detection with LipidTOX™ Red

H1299-eGFP cells were seeded (75000 cells/compartment) and were allowed to settle overnight as specified for the AF647 ON release experiment. Next, the cells were incubated with a mixture of a 1/1000 dilution of the LipidTOX™ Red Phospholipidosis Detection Reagent (Thermo Fisher Scientific, Rockford, USA) and the desired compounds in CCM. Upon 20 h

incubation, the nuclei were labeled with Hoechst 33342 as detailed for the AF647 ON release experiment. The 408 nm, 488 nm and 561 nm laser lines were applied to, respectively, excite the Hoechst labeled nuclei, the eGFP protein and the fluorescence resulting from the LipidTOX™ Red Phospholipidosis dye. Imaging occurred with a SDC microscope as described above for visualizing the cytosolic release of AF647 ONs with confocal microscopy. The LipidTOX™ Red Phospholipidosis signal area was determined with ImageJ (FIJI) in at least 175 cells from minimum 41 images. To this end, all confocal images were processed by applying the same offset values for the LipidTOX™ Red Phospholipidosis signal. In each image, both the number of cells and signal area of the LipidTOX™ Red Phospholipidosis dye was determined to allow calculation of the normalized LipidTOX™ Red Phospholipidosis area (*i.e.* LipidTOX™ Red Phospholipidosis signal area/cell number) in each image. The fold change in LipidTOX™ Red Phospholipidosis signal area was calculated by dividing the normalized signal area in treated cells by the normalized signal area in untreated cells.

Visualizing lysosomes

H1299-eGFP cells were seeded as specified for the AF647 ON release and LipidTOX™ experiment and subsequently treated with the indicated compound concentrations for 20 h. Next, after removal of the compound-containing CCM, lysosomes and nuclei were labeled with, respectively, 75 nM LysoTracker™ Deep Red (LDR) and Hoechst 33342 in CCM (1 mg/mL in water, 1/1000 dilution) during 30 min at 37 °C. Finally, following dye removal, fresh CCM was added and cells were kept at 37 °C in a humidified atmosphere containing 5% CO_2 until imaging (no fixation step was applied). A laser scanning confocal microscope (Nikon A1R HD confocal, Nikon, Japan), equipped with a Plan Apo VC 60× 1.4 NA oil immersion objective lens (Nikon, Japan), a resonant scanner and NIS Elements software (Nikon, Japan) was applied for imaging. The 405 nm, 488 nm and 640 nm laser lines were applied to, respectively, excite the Hoechst labeled nuclei, the eGFP protein and the fluorescence resulting from the LDR-stained lysosomes.

Statistical analysis

Statistical analysis was performed using the 6th version of the GraphPad Prism software. One-way ANOVA combined with the post-hoc Dunnett test was applied to compare multiple conditions, whereas the student *t*-test was used for direct comparison of 2 conditions. Multiple linear regression analysis was performed with normalized eGFP expression as a dependent variable. A p value ≤ 0.05 was considered *a priori* to be statistically significant.

Associated content

Supporting information consists out of 9 additional figures (Figure S1-S9), 2 additional tables (Table S1-S2), and a supplementary materials and methods section.

Author information

Prof. Dr. Koen Raemdonck

Ghent Research Group on Nanomedicines, Laboratory of General Biochemistry and Physical Pharmacy

Department of Pharmaceutics

Ghent University

Ottergemsesteenweg 460, 9000 Ghent

Belgium

Telephone: +32 9 264 80 78

Fax: +32 9 264 81 89

Email address: Koen.Raemdonck@UGent.be

Author Contributions

The manuscript was written through contributions of all authors. All authors have given approval to the final version of the manuscript.

Notes

The authors declare no competing financial interest.

ACKNOWLEDGMENTS

T.V.d.V is a doctoral fellow of the Research Foundation-Flanders (grant 1198719N, FWO, Belgium). L.D.B. acknowledges the Special Research Fund of Ghent University (BOF12/GOA/014). I.E. is a PhD student in the CDIT laboratory and holds PhD fellowship from FWO-Flanders (11F7723N). K.R. and C.M. acknowledge the Research Foundation Flanders (FWO) for funding through research grant G039419N. K.R. additionally acknowledges the European Research Council (ERC) for funding received under the European Union's Horizon 2020 research and innovation program (Grant agreement No. 101002571). We thank Prof. R. Vandenbroucke from the VIB-UGent Center for Inflammation Research (Ghent, Belgium) for the use of the microfluidic NanoAssemblr® Benchtop mixing device.

REFERENCES

[1] X. Shen, D.R. Corey, Chemistry, mechanism and clinical status of antisense oligonucleotides and duplex RNAs, Nucleic Acids Res. 46 (2018) 1584–1600. https://doi.org/10.1093/nar/gkx1239.

[2] A. Wittrup, J. Lieberman, Knocking down disease: a progress report on siRNA therapeutics, Nat Rev Genet. 16 (2015) 543–552. https://doi.org/10.1038/nrg3978.

[3] S.F. Dowdy, Overcoming cellular barriers for RNA therapeutics, Nat Biotechnol. 35 (2017) 222–229. https://doi.org/10.1038/nbt.3802.

[4] A. Fire, S. Xu, M.K. Montgomery, S.A. Kostas, S.E. Driver, C.C. Mello, Potent and specific genetic interference by double-stranded RNA in caenorhabditis elegans, Nature. 391 (1998) 806–811. https://doi.org/10.1038/35888.

[5] T.F. Martens, K. Remaut, J. Demeester, S.C. De Smedt, K. Braeckmans, Intracellular delivery of nanomaterials: How to catch endosomal escape in the act, Nano Today. 9 (2014) 344–364. https://doi.org/10.1016/j.nantod.2014.04.011.

[6] K. Raemdonck, R.E. Vandenbroucke, J. Demeester, N.N. Sanders, S.C. De Smedt, Maintaining the silence: reflections on long-term RNAi, Drug Discov Today. 13 (2008) 917–931. https://doi.org/10.1016/j.drudis.2008.06.008.

[7] S.M. Hoy, Patisiran: First Global Approval, Drugs. 78 (2018) 1625–1631. https://doi.org/10.1007/s40265-018-0983-6.

[8] A. Akinc, M.A. Maier, M. Manoharan, K. Fitzgerald, M. Jayaraman, S. Barros, S. Ansell, X. Du, M.J. Hope, T.D. Madden, B.L. Mui, S.C. Semple, Y.K. Tam, M. Ciufolini, D. Witzigmann, J.A. Kulkarni, R. van der Meel, P.R. Cullis, The Onpattro story and the clinical translation of nanomedicines containing nucleic acid-based drugs, Nat Nanotechnol. 14 (2019) 1084–1087. https://doi.org/10.1038/s41565-019-0591-y.

[9] S. Garrelfs, Y. Frishberg, S. Hulton, M. Koren, W. O'Riordan, P. Cochat, G. Deschenes, H. Shasha-Lavsky, J. Saland, W. Van't Hoff, D.G. Fuster, D. Magen, S. Moochhala, G. Schalk, E. Simkova, J. Groothoff, D. Sas, K. Meliambro, J. Lu, P. Garg, J. Gansner, T. McGregor, J. Lieske, LB002ILLUMINATE-A, A PHASE 3 STUDY OF LUMASIRAN, AN INVESTIGATIONAL RNAI THERAPEUTIC, IN CHILDREN AND ADULTS WITH PRIMARY HYPEROXALURIA TYPE 1 (PH1), Nephrology Dialysis Transplantation. 35 (2020) gfaa146.LB002. https://doi.org/10.1093/ndt/gfaa146.lb002.

[10] M. Balwani, E. Sardh, P. Ventura, P.A. Peiró, D.C. Rees, U. Stölzel, D.M. Bissell, H.L. Bonkovsky, J. Windyga, K.E. Anderson, C. Parker, S.M. Silver, S.B. Keel, J.-D. Wang, P.E. Stein, P. Harper, D. Vassiliou, B. Wang, J. Phillips, A. Ivanova, J.G. Langendonk, R. Kauppinen, E. Minder, Y. Horie, C. Penz, J. Chen, S. Liu, J.J. Ko, M.T. Sweetser, P. Garg, A. Vaishnaw, J.B. Kim, A.R. Simon, L. Gouya, Phase 3 Trial of RNAi Therapeutic Givosiran for Acute Intermittent Porphyria, New England Journal of Medicine. 382 (2020) 2289–2301. https://doi.org/10.1056/NEJMoa1913147.

[11] R. Kanasty, J.R. Dorkin, A. Vegas, D. Anderson, Delivery materials for siRNA therapeutics, Nat Mater. 12 (2013) 967–977. https://doi.org/10.1038/nmat3765.

[12] H. Yin, R.L. Kanasty, A.A. Eltoukhy, A.J. Vegas, J.R. Dorkin, D.G. Anderson, Non-viral vectors for gene-based therapy, Nat Rev Genet. 15 (2014) 541–555. https://doi.org/10.1038/nrg3763.

[13] C.R. Brown, S. Gupta, J. Qin, T. Racie, G. He, S. Lentini, R. Malone, M. Yu, S. Matsuda, S. Shulga-Morskaya, A. V Nair, C.S. Theile, K. Schmidt, A. Shahraz, V. Goel, R.G. Parmar, I. Zlatev, M.K. Schlegel, J.K. Nair, M. Jayaraman, M. Manoharan, D. Brown, M.A. Maier, V. Jadhav, Investigating the pharmacodynamic durability of GalNAc–siRNA conjugates, Nucleic Acids Res. (2020) gkaa670. https://doi.org/10.1093/nar/gkaa670.

[14] K. Raemdonck, B. Naeye, K. Buyens, R.E. Vandenbroucke, A. Høgset, J. Demeester, S.C. De Smedt, Biodegradable Dextran Nanogels for RNA Interference: Focusing on Endosomal Escape and Intracellular siRNA Delivery, Adv Funct Mater. 19 (2009) 1406–1415. https://doi.org/10.1002/adfm.200801795.

[15] M. Hirsch, M. Helm, Live cell imaging of duplex siRNA intracellular trafficking, Nucleic Acids Res. 43 (2015) 4650–4660. https://doi.org/10.1093/nar/gkv307.

[16] S.T. Crooke, S. Wang, T.A. Vickers, W. Shen, X. Liang, Cellular uptake and trafficking of antisense oligonucleotides, Nat Biotechnol. 35 (2017) 230–237. https://doi.org/10.1038/nbt.3779.

[17] A. Wittrup, A. Ai, X. Liu, P. Hamar, R. Trifonova, K. Charisse, M. Manoharan, T. Kirchhausen, J. Lieberman, Visualizing lipid-formulated siRNA release from endosomes and target gene knockdown, Nat Biotechnol. 33 (2015) 870–876. https://doi.org/10.1038/nbt.3298.

[18] J. Gilleron, W. Querbes, A. Zeigerer, A. Borodovsky, G. Marsico, U. Schubert, K. Manygoats, S. Seifert, C. Andree, M. Stöter, H. Epstein-Barash, L. Zhang, V. Koteliansky, K. Fitzgerald, E. Fava, M. Bickle, Y. Kalaidzidis, A. Akinc, M. Maier, M. Zerial, Image-based analysis of lipid nanoparticle-mediated siRNA delivery, intracellular trafficking and endosomal escape, Nat Biotechnol. 31 (2013) 638–646. https://doi.org/10.1038/nbt.2612.

[19] G. Sahay, W. Querbes, C. Alabi, A. Eltoukhy, S. Sarkar, C. Zurenko, E. Karagiannis, K. Love, D. Chen, R. Zoncu, Y. Buganim, A. Schroeder, R. Langer, D.G. Anderson, Efficiency of siRNA delivery by lipid nanoparticles is limited by endocytic recycling, Nat Biotechnol. 31 (2013) 653–658. https://doi.org/10.1038/nbt.2614.

[20] A.D. Springer, S.F. Dowdy, GalNAc-siRNA Conjugates: Leading the Way for Delivery of RNAi Therapeutics, Nucleic Acid Ther. 28 (2018) 109–118. https://doi.org/10.1089/nat.2018.0736.

[21] D. Ma, Enhancing endosomal escape for nanoparticle mediated siRNA delivery, Nanoscale. 6 (2014) 6415–6424. https://doi.org/10.1039/c4nr00018h.

[22] T. Van de Vyver, S.C. De Smedt, K. Raemdonck, Modulating intracellular pathways to improve non-viral delivery of RNA therapeutics, Adv Drug Deliv Rev. 181 (2022) 114041. https://doi.org/10.1016/J.ADDR.2021.114041.

[23] B. Bogaert, F. Sauvage, R. Guagliardo, C. Muntean, V.P. Nguyen, E. Pottie, M. Wels, A.-K. Minnaert, R. De Rycke, Q. Yang, D. Peer, N. Sanders, K. Remaut, Y.M. Paulus, C. Stove, S.C. De Smedt, K. Raemdonck, A lipid nanoparticle platform for mRNA delivery through repurposing of cationic amphiphilic drugs, Journal of Controlled Release. 350 (2022) 256–270. https://doi.org/10.1016/j.jconrel.2022.08.009.

[24] F. Joris, S.C. De Smedt, K. Raemdonck, Small molecules convey big messages: Boosting non-viral nucleic acid delivery with low molecular weight drugs, Nano Today. 16 (2017) 14–29. https://doi.org/10.1016/j.nantod.2017.06.012.

[25] T. Van de Vyver, B. Bogaert, L. De Backer, F. Joris, R. Guagliardo, J. Van Hoeck, P. Merckx, S. Van Calenbergh, S. Ramishetti, D. Peer, K. Remaut, S.C. De Smedt, K. Raemdonck, Cationic Amphiphilic Drugs Boost the Lysosomal Escape of Small Nucleic Acid Therapeutics in a Nanocarrier-Dependent Manner, ACS Nano. 14 (2020) 4774–4791. https://doi.org/10.1021/acsnano.0c00666.

[26] E. Shaabani, M. Sharifiaghdam, J. Lammens, H. De Keersmaecker, C. Vervaet, T. De Beer, E. Motevaseli, M.H. Ghahremani, P. Mansouri, S. De Smedt, K. Raemdonck, R. Faridi-Majidi, K. Braeckmans, J.C. Fraire, Increasing angiogenesis factors in hypoxic diabetic wound conditions by sirna delivery: Additive effect of lbl-gold nanocarriers and desloratadine-induced lysosomal escape, Int J Mol Sci. (2021). https://doi.org/10.3390/ijms22179216.

[27] F. Joris, L. De Backer, T. Van de Vyver, C. Bastiancich, S.C. De Smedt, K. Raemdonck, Repurposing cationic amphiphilic drugs as adjuvants to induce lysosomal siRNA escape in nanogel transfected cells, Journal of Controlled Release. 269 (2018) 266–276. https://doi.org/10.1016/j.jconrel.2017.11.019.

[28] J. Kornhuber, P. Tripal, M. Reichel, L. Terfloth, S. Bleich, J. Wiltfang, E. Gulbins, Identification of new functional inhibitors of acid sphingomyelinase using a structure-property-activity relation model, J Med Chem. 51 (2008) 219–237. https://doi.org/10.1021/jm070524a.

[29] J. Kornhuber, M. Muehlbacher, S. Trapp, S. Pechmann, A. Friedl, M. Reichel, C. Mühle, L. Terfloth, T.W. Groemer, G.M. Spitzer, K.R. Liedl, E. Gulbins, P. Tripal, Identification of novel functional inhibitors of acid sphingomyelinase., PLoS One. 6 (2011) e23852. https://doi.org/10.1371/journal.pone.0023852.

[30] L. Goracci, M. Ceccarelli, D. Bonelli, G. Cruciani, Modeling Phospholipidosis Induction: Reliability and Warnings, J Chem Inf Model. 53 (2013) 1436–1446. https://doi.org/10.1021/ci400113t.

[31] M. Muehlbacher, P. Tripal, F. Roas, J. Kornhuber, Identification of Drugs Inducing Phospholipidosis by Novel *In vitro* Data, ChemMedChem. 7 (2012) 1925–1934. https://doi.org/10.1002/cmdc.201200306.

[32] R.S. Funk, J.P. Krise, Cationic amphiphilic drugs cause a marked expansion of apparent lysosomal volume: Implications for an intracellular distribution-based drug interaction, Mol Pharm. 9 (2012) 1384–1395. https://doi.org/10.1021/mp200641e.

[33] R. Logan, A.C. Kong, E. Axcell, J.P. Krise, Amine-containing molecules and the induction of an expanded lysosomal volume phenotype: A structure-activity relationship study, J Pharm Sci. 103 (2014) 1572–1580. https://doi.org/10.1002/jps.23949.

[34] N.H.T. Petersen, O.D. Olsen, L. Groth-Pedersen, A.-M. Ellegaard, M. Bilgin, S. Redmer, M.S. Ostenfeld, D. Ulanet, T.H. Dovmark, A. Lønborg, S.D. Vindeløv, D. Hanahan, C. Arenz, C.S. Ejsing, T. Kirkegaard, M. Rohde, J. Nylandsted, M. Jäättelä, Transformation-Associated Changes in Sphingolipid Metabolism Sensitize Cells to Lysosomal Cell Death Induced by Inhibitors of Acid Sphingomyelinase, Cancer Cell. 24 (2013) 379–393. https://doi.org/10.1016/j.ccr.2013.08.003.

[35] E. Gulbins, R.N. Kolesnick, It takes a CAD to kill a tumor cell with a LMP., Cancer Cell. 24 (2013) 279–81. https://doi.org/10.1016/j.ccr.2013.08.025.

[36] R. Fuchs, A. Stracke, N. Ebner, C.W. Zeller, A.M. Raninger, M. Schittmayer, T. Kueznik, M. Absenger-Novak, R. Birner-Gruenberger, The cytotoxicity of the α1-adrenoceptor antagonist prazosin is linked to an endocytotic mechanism equivalent to transport-P, Toxicology. 338 (2015) 17–29. https://doi.org/10.1016/J.TOX.2015.09.008.

[37] R. Fuchs, A. Stracke, V. Holzmann, G. Luschin-Ebengreuth, N. Meier-Allard, N. Ebner, T.M. Lassacher, M. Absenger-Novak, E. Fröhlich, M. Schittmayer, S. Cano Crespo, M. Palacin, B. Rinner, R. Birner-Gruenberger, Prazosin induced lysosomal tubulation interferes with cytokinesis and the endocytic sorting of the tumour antigen CD98hc, Biochimica et Biophysica Acta (BBA) - Molecular Cell Research. 1865 (2018) 1211–1229. https://doi.org/10.1016/J.BBAMCR.2018.06.006.

[38] R. Fuchs, I. Stelzer, H.S. Haas, G. Leitinger, K. Schauenstein, A. Sadjak, The α1-adrenergic receptor antagonists, benoxathian and prazosin, induce apoptosis and a switch towards megakaryocytic differentiation in human erythroleukemia cells, Ann Hematol. 88 (2009) 989–997. https://doi.org/10.1007/s00277-009-0704-z.

[39] R. Fuchs, E. Schraml, G. Leitinger, I. Stelzer, N. Allard, H.S. Haas, K. Schauenstein, A. Sadjak, α1-adrenergic drugs modulate differentiation and cell death of human

erythroleukemia cells through non adrenergic mechanism, Exp Cell Res. 317 (2011) 2239–2251. https://doi.org/10.1016/j.yexcr.2011.07.005.

[40] R. Fuchs, G. Schwach, A. Stracke, N. Meier-Allard, M. Absenger, E. Ingolic, H.S. Haas, R. Pfragner, A. Sadjak, The anti-hypertensive drug prazosin induces apoptosis in the medullary thyroid carcinoma cell line TT., Anticancer Res. 35 (2015) 31–38.

[41] S.C. Lin, S.C. Chueh, C.J. Hsiao, T.K. Li, T.H. Chen, C.H. Liao, P.C. Lyu, J.H. Guh, Prazosin displays anticancer activity against human prostate cancers: Targeting DNA and cell cycle, Neoplasia. 9 (2007) 830–839. https://doi.org/10.1593/neo.07475.

[42] S. Assad Kahn, S.L. Costa, S. Gholamin, R.T. Nitta, L.G. Dubois, M. Fève, M. Zeniou, P.L.C. Coelho, E. El-Habr, J. Cadusseau, P. Varlet, S.S. Mitra, B. Devaux, M. Kilhoffer, S.H. Cheshier, V. Moura-Neto, J. Haiech, M. Junier, H. Chneiweiss, The anti-hypertensive drug prazosin inhibits glioblastoma growth via the PKCδ-dependent inhibition of the AKT pathway, EMBO Mol Med. 8 (2016) 511–526. https://doi.org/10.15252/emmm.201505421.

[43] A. Forbes, S. Anoopkumar-Dukie, R. Chess-Williams, C. McDermott, Relative cytotoxic potencies and cell death mechanisms of α_1-adrenoceptor antagonists in prostate cancer cell lines, Prostate. 76 (2016) 757–766. https://doi.org/10.1002/pros.23167.

[44] J. Zhang, J. Fan, Prazosin inhibits the proliferation, migration and invasion, but promotes the apoptosis of U251 and U87 cells via the PI3K/AKT/mTOR signaling pathway, Exp Ther Med. 20 (2020) 1145–1152. https://doi.org/10.3892/etm.2020.8772.

[45] X. Sun, S. Yang, W. Song, Prazosin inhibits the proliferation and survival of acute myeloid leukaemia cells through down-regulating TNS1, Biomedicine and Pharmacotherapy. 124 (2020) 109731. https://doi.org/10.1016/j.biopha.2019.109731.

[46] P. Kozik, M. Gros, D.N. Itzhak, L. Joannas, S. Heurtebise-Chrétien, P.A. Krawczyk, P. Rodríguez-Silvestre, A. Alloatti, J.G. Magalhaes, E. Del Nery, G.H.H. Borner, S. Amigorena, Small Molecule Enhancers of Endosome-to-Cytosol Import Augment Anti-tumor Immunity, Cell Rep. 32 (2020) 107905. https://doi.org/10.1016/j.celrep.2020.107905.

[47] V.D. Turubanova, I. V. Balalaeva, T.A. Mishchenko, E. Catanzaro, R. Alzeibak, N.N. Peskova, I. Efimova, C. Bachert, E. V. Mitroshina, O. Krysko, M. V. Vedunova, D. V. Krysko, Immunogenic cell death induced by a new photodynamic therapy based on photosens and photodithazine, J Immunother Cancer. 7 (2019) 350. https://doi.org/10.1186/s40425-019-0826-3.

[48] N. Yatim, S. Cullen, M.L. Albert, Dying cells actively regulate adaptive immune responses, Nat Rev Immunol. 17 (2017) 262–275. https://doi.org/10.1038/nri.2017.9.

[49] S. Lepri, A. Valeri, S. Buratta, M. Ceccarelli, D. Bartolini, R. Ruzziconi, L. Goracci, Synthesis and phospholipidosis effect of a series of cationic amphiphilic compounds: a case study to evaluate *In silico* and *In vitro* assays, Medicinal Chemistry Research. 27 (2018) 679–692. https://doi.org/10.1007/s00044-017-2093-5.

[50] J.Y. Choe, D.S. Son, Y. Kim, J. Lee, H. Shin, W.J. Kim, Y.G. Kang, P. Dua, S.W. Hong, J.H. Park, D. Lee, L-Type Calcium Channel Blocker Enhances Cellular Delivery and Gene Silencing Potency of Cell-Penetrating Asymmetric siRNAs, Mol Pharm. 17 (2020) 777–786. https://doi.org/10.1021/acs.molpharmaceut.9b00942.

[51] J. Lamb, E.D. Crawford, D. Peck, J.W. Modell, I.C. Blat, M.J. Wrobel, J. Lerner, J.P. Brunet, A. Subramanian, K.N. Ross, M. Reich, H. Hieronymus, G. Wei, S.A. Armstrong, S.J. Haggarty, P.A. Clemons, R. Wei, S.A. Carr, E.S. Lander, T.R. Golub, The connectivity map: Using gene-expression signatures to connect small molecules, genes, and disease, Science (1979). 313 (2006) 1929–1935. https://doi.org/10.1126/science.1132939.

[52] F. Sirci, F. Napolitano, S. Pisonero-Vaquero, D. Carrella, D.L. Medina, D. di Bernardo, Comparing structural and transcriptional drug networks reveals signatures of drug activity and toxicity in transcriptional responses, NPJ Syst Biol Appl. 3 (2017) 23. https://doi.org/10.1038/s41540-017-0022-3.

[53] L. Wang, R.C. MacDonald, Effects of microtubule-depolymerizing agents on the transfection of cultured vascular smooth muscle cells: Enhanced expression with free drug and especially with drug-gene lipoplexes, Molecular Therapy. 9 (2004) 729–737. https://doi.org/10.1016/j.ymthe.2004.02.009.

[54] R.R. Nair, J.R. Rodgers, L.A. Schwarz, Enhancement of transgene expression by combining glucocorticoids and anti-mitotic agents during transient transfection using DNA-cationic liposomes, Molecular Therapy. 5 (2002) 455–462. https://doi.org/10.1006/mthe.2002.0567.

[55] N.R. Chowdhury, R.M. Hays, V.R. Bommineni, N. Franki, J.R. Chowdhury, C.H. Wu, G.Y. Wu, Microtubular disruption prolongs the expression of human bilirubin-uridinediphosphoglucuronate-glucuronosyltransferase-1 gene transferred into gunn rat livers, Journal of Biological Chemistry. 271 (1996) 2341–2346. https://doi.org/10.1074/jbc.271.4.2341.

[56] J. Lindberg, M.A.M. Fernandez, J.D. Ropp, S.F. Hamm-Alvarez, Nocodazole treatment of CV-1 cells enhances nuclear/perinuclear accumulation of lipid-DNA complexes and increases gene expression, Pharm Res. 18 (2001) 246–249. https://doi.org/10.1023/A:1011001022570.

[57] F. Cardarelli, L. Digiacomo, C. Marchini, A. Amici, F. Salomone, G. Fiume, A. Rossetta, E. Gratton, D. Pozzi, G. Caracciolo, The intracellular trafficking mechanism of

Lipofectamine-based transfection reagents and its implication for gene delivery, Sci Rep. 6 (2016) 25879. https://doi.org/10.1038/srep25879.

[58] S. Hasegawa, N. Hirashima, M. Nakanishi, Microtubule involvement in the intracellular dynamics for gene trasnfection mediated by cationic liposomes, Gene Ther. 8 (2001) 1669–1673. https://doi.org/10.1038/sj.gt.3301573.

[59] D.S. Wishart, C. Knox, A.C. Guo, S. Shrivastava, M. Hassanali, P. Stothard, Z. Chang, J. Woolsey, DrugBank: a comprehensive resource for *In silico* drug discovery and exploration., Nucleic Acids Res. 34 (2006) D668-72. https://doi.org/10.1093/nar/gkj067.

[60] J. Symersky, D. Osowski, D.E. Walters, D.M. Mueller, Oligomycin frames a common drug-binding site in the ATP synthase, Proc Natl Acad Sci U S A. 109 (2012) 13961–13965. https://doi.org/10.1073/pnas.1207912109.

[61] I. Shrestha, J.S. Choi, Y.U. Bae, K.O. Doh, Enhancement of Liposomal Plasmid DNA and siRNA Delivery by Itraconazole through Intracellular Cholesterol Accumulation, Pharm Res. 37 (2020) 1–9. https://doi.org/10.1007/s11095-020-02846-4.

[62] M.N. Trinha, F. Lua, X. Lib, A. Dasa, Q. Liangd, J.K. De Brabanderd, M.S. Browna, J.L. Goldsteina, Triazoles inhibit cholesterol export from lysosomes by binding to NPC1, Proc Natl Acad Sci U S A. 114 (2017) 89–94. https://doi.org/10.1073/pnas.1619571114.

[63] S.A. Head, W.Q. Shi, E.J. Yang, B.A. Nacev, S.Y. Hong, K.K. Pasunooti, R.J. Li, J.S. Shim, J.O. Liu, Simultaneous targeting of NPC1 and VDAC1 by itraconazole leads to synergistic inhibition of MTOR signaling and angiogenesis, ACS Chem Biol. 12 (2017) 174–182. https://doi.org/10.1021/acschembio.6b00849.

[64] H. Wang, Y.Y.C. Tam, S. Chen, J. Zaifman, R. Van Der Meel, M.A. Ciufolini, P.R. Cullis, The niemann-pick C1 inhibitor NP3.47 enhances gene silencing potency of lipid nanoparticles containing siRNA, Molecular Therapy. 24 (2016) 2100–2108. https://doi.org/10.1038/mt.2016.179.

[65] S.M. Corsello, J.A. Bittker, Z. Liu, J. Gould, P. McCarren, J.E. Hirschman, S.E. Johnston, A. Vrcic, B. Wong, M. Khan, J. Asiedu, R. Narayan, C.C. Mader, A. Subramanian, T.R. Golub, The Drug Repurposing Hub: a next-generation drug library and information resource, Nat Med. 23 (2017) 405–408. https://doi.org/10.1038/nm.4306.

[66] J. Surre, C. Saint-Ruf, V. Collin, S. Orenga, M. Ramjeet, I. Matic, Strong increase in the autofluorescence of cells signals struggle for survival, Sci Rep. 8 (2018) 12088. https://doi.org/10.1038/s41598-018-30623-2.

[67] E. de Nadal, G. Ammerer, F. Posas, Controlling gene expression in response to stress, Nat Rev Genet. 12 (2011) 833–845. https://doi.org/10.1038/nrg3055.

[68] *JChem for Office (Excel)*, version 17.21.0.1797; Software was used for chemical database access, structure based property calculation, search and reporting; ChemAxon: Budapest, Hungary, 2017. http://www.chemaxon.com, (n.d.).

[69] L.M.P. Vermeulen, T. Brans, S.K. Samal, P. Dubruel, J. Demeester, S.C. De Smedt, K. Remaut, K. Braeckmans, Endosomal Size and Membrane Leakiness Influence Proton Sponge-Based Rupture of Endosomal Vesicles, ACS Nano. 12 (2018) 2332–2345. https://doi.org/10.1021/acsnano.7b07583.

[70] Z. ur Rehman, D. Hoekstra, I.S. Zuhorn, Mechanism of Polyplex- and Lipoplex-Mediated Delivery of Nucleic Acids: Real-Time Visualization of Transient Membrane Destabilization without Endosomal Lysis, ACS Nano. 7 (2013) 3767–3777. https://doi.org/10.1021/nn3049494.

[71] H. Du Rietz, H. Hedlund, S. Wilhelmson, P. Nordenfelt, A. Wittrup, Imaging small molecule-induced endosomal escape of siRNA, Nat Commun. 11 (2020) 1809. https://doi.org/10.1038/s41467-020-15300-1.

[72] M.L. MacDonald, J. Lamerdin, S. Owens, B.H. Keon, G.K. Bilter, Z. Shang, Z. Huang, H. Yu, J. Dias, T. Minami, S.W. Michnick, J.K. Westwick, Identifying off-target effects and hidden phenotypes of drugs in human cells, Nat Chem Biol. 2 (2006) 329–337. https://doi.org/10.1038/nchembio790.

[73] J.F.M. da Silva, M. Walters, S. Al-Damluji, C.R. Ganellin, Molecular features of the prazosin molecule required for activation of Transport-P, Bioorg Med Chem. 16 (2008) 7254–7263. https://doi.org/10.1016/j.bmc.2008.06.037.

[74] L. De Backer, K. Braeckmans, M.C.A. Stuart, J. Demeester, S.C. De Smedt, K. Raemdonck, Bio-inspired pulmonary surfactant-modified nanogels: A promising siRNA delivery system, Journal of Controlled Release. 206 (2015) 177–186. https://doi.org/10.1016/j.jconrel.2015.03.015.

[75] X. Zhang, W. Wang, A. V. Bedigian, M.L. Coughlin, T.J. Mitchison, U.S. Eggert, Dopamine receptor D3 regulates endocytic sorting by a Prazosin-sensitive interaction with the coatomer COPI, Proc Natl Acad Sci U S A. 109 (2012) 12485–12490. https://doi.org/10.1073/pnas.1207821109.

[76] R. Fuchs, E. Schraml, G. Leitinger, I. Letofsky-Papst, I. Stelzer, H.S. Haas, K. Schauenstein, A. Sadjak, α1-adrenergic drugs exhibit affinity to a thapsigargin-sensitive binding site and interfere with the intracellular Ca2+ homeostasis in human erythroleukemia cells, Exp Cell Res. 317 (2011) 2969–2980. https://doi.org/10.1016/j.yexcr.2011.08.003.

[77] J.R. González-Juanatey, M.J. Iglesias, C. Alcaide, R. Piñeiro, F. Lago, Doxazosin induces apoptosis in cardiomyocytes cultured in vitro by a mechanism that is independent of

α1-adrenergic blockade, Circulation. 107 (2003) 127–131. https://doi.org/10.1161/01.CIR.0000043803.20822.D1.

[78] X. Cai, Y. Xu, A.K. Cheung, R.C. Tomlinson, A. Alcázar-Román, L. Murphy, A. Billich, B. Zhang, Y. Feng, M. Klumpp, J.M. Rondeau, A.N. Fazal, C.J. Wilson, V. Myer, G. Joberty, T. Bouwmeester, M.A. Labow, P.M. Finan, J.A. Porter, H.L. Ploegh, D. Baird, P. De Camilli, J.A. Tallarico, Q. Huang, PIKfyve, a class III PI Kinase, is the target of the small molecular IL-12/IL-23 inhibitor apilimod and a player in toll-like receptor signaling, Chem Biol. 20 (2013) 912–921. https://doi.org/10.1016/j.chembiol.2013.05.010.

[79] K. Fogarty, M. Kashem, A. Bauer, A. Bernardino, D. Brennan, B. Cook, N. Farrow, T. Molinaro, R. Nelson, Development of Three Orthogonal Assays Suitable for the Identification and Qualification of PIKfyve Inhibitors, Assay Drug Dev Technol. 15 (2017) 210–219. https://doi.org/10.1089/adt.2017.790.

[80] O. Sano, K. Kazetani, M. Funata, Y. Fukuda, J. Matsui, H. Iwata, Vacuolin-1 inhibits autophagy by impairing lysosomal maturation via PIKfyve inhibition, FEBS Lett. 590 (2016) 1576–1585. https://doi.org/10.1002/1873-3468.12195.

[81] H.B.J. Jefferies, F.T. Cooke, P. Jat, C. Boucheron, T. Koizumi, M. Hayakawa, H. Kaizawa, T. Ohishi, P. Workman, M.D. Waterfield, P.J. Parker, A selective PIKfyve inhibitor blocks PtdIns(3,5)P_2 production and disrupts endomembrane transport and retroviral budding, EMBO Rep. 9 (2008) 164–170. https://doi.org/10.1038/sj.embor.7401155.

[82] N. Hayakawa, M. Noguchi, S. Takeshita, A. Eviryanti, Y. Seki, H. Nishio, R. Yokoyama, M. Noguchi, M. Shuto, Y. Shima, K. Kuribayashi, S. Kageyama, H. Eda, M. Suzuki, T. Hatta, S. Iemura, T. Natsume, I. Tanabe, R. Nakagawa, M. Shiozaki, K. Sakurai, M. Shoji, A. Andou, T. Yamamoto, Structure–activity relationship study, target identification, and pharmacological characterization of a small molecular IL-12/23 inhibitor, APY0201, Bioorg Med Chem. 22 (2014) 3021–3029. https://doi.org/10.1016/J.BMC.2014.03.036.

[83] Y.L. Kang, Y.Y. Chou, P.W. Rothlauf, Z. Liu, T.K. Soh, D. Cureton, J.B. Case, R.E. Chen, M.S. Diamond, S.P.J. Whelan, T. Kirchhausen, Inhibition of PIKfyve kinase prevents infection by Zaire ebolavirus and SARS-CoV-2, Proc Natl Acad Sci U S A. 117 (2020) 20803–20813. https://doi.org/10.1073/pnas.2007837117.

[84] D. Sbrissa, G. Naisan, O.C. Ikonomov, A. Shisheva, Apilimod, a candidate anticancer therapeutic, arrests not only PtdIns(3,5)P2 but also PtdIns5P synthesis by PIKfyve and induces bafilomycin A1-reversible aberrant endomembrane dilation, PLoS One. 13 (2018) e0204532. https://doi.org/10.1371/journal.pone.0204532.

[85] R.M. Dayam, C.X. Sun, C.H. Choy, G. Mancuso, M. Glogauer, R.J. Botelho, The Lipid Kinase PIKfyve Coordinates the Neutrophil Immune Response through the Activation of the Rac GTPase, The Journal of Immunology. 199 (2017) 2096–2105. https://doi.org/10.4049/jimmunol.1601466.

[86] M. V. Baranov, F. Bianchi, A. Schirmacher, M.A.C. van Aart, S. Maassen, E.M. Muntjewerff, I. Dingjan, M. ter Beest, M. Verdoes, S.G.L. Keyser, C.R. Bertozzi, U. Diederichsen, G. van den Bogaart, The Phosphoinositide Kinase PIKfyve Promotes Cathepsin-S-Mediated Major Histocompatibility Complex Class II Antigen Presentation, IScience. 11 (2019) 160–177. https://doi.org/10.1016/j.isci.2018.12.015.

[87] S. Gayle, S. Landrette, N. Beeharry, C. Conrad, M. Hernandez, P. Beckett, S.M. Ferguson, T. Mandelkern, M. Zheng, T. Xu, J. Rothberg, H. Lichenstein, Identification of apilimod as a first-in-class PIKfyve kinase inhibitor for treatment of B-cell non-Hodgkin lymphoma, Blood. 129 (2017) 1768–1778. https://doi.org/10.1182/blood-2016-09-736892.

[88] Y. Lu, S. Dong, B. Hao, C. Li, K. Zhu, W. Guo, Q. Wang, K.H. Cheung, C.W.M. Wong, W.T. Wu, H. Markus, J. Yue, Vacuolin-1 potently and reversibly inhibits autophagosome-lysosome fusion by activating RAB5A, Autophagy. 10 (2014) 1895–1905. https://doi.org/10.4161/auto.32200.

[89] C. Chen, Y. Lu, H.M. Siu, J. Guan, L. Zhu, S. Zhang, J. Yue, L. Zhang, Identification of Novel Vacuolin-1 Analogues as Autophagy Inhibitors by Virtual Drug Screening and Chemical Synthesis, Molecules. 22 (2017) 891. https://doi.org/10.3390/molecules22060891.

[90] J. Cerny, Y. Feng, A. Yu, K. Miyake, B. Borgonovo, J. Klumperman, J. Meldolesi, P.L. McNeil, T. Kirchhausen, The small chemical vacuolin-1 inhibits Ca2+-dependent lysosomal exocytosis but not cell resealing, EMBO Rep. 5 (2004) 883–888. https://doi.org/10.1038/sj.embor.7400243.

[91] G.H.E. Kim, R.M. Dayam, A. Prashar, M. Terebiznik, R.J. Botelho, PIKfyve Inhibition Interferes with Phagosome and Endosome Maturation in Macrophages, Traffic. 15 (2014) 1143–1163. https://doi.org/10.1111/tra.12199.

[92] A.C. Rutherford, C. Traer, T. Wassmer, K. Pattni, M. V. Bujny, J.G. Carlton, H. Stenmark, P.J. Cullen, The mammalian phosphatidylinositol 3-phosphate 5-kinase (PIKfyve) regulates endosome-to-TGN retrograde transport, J Cell Sci. 119 (2006) 3944–3957. https://doi.org/10.1242/jcs.03153.

[93] M.F. Osborn, A.H. Coles, A. Biscans, R.A. Haraszti, L. Roux, S. Davis, S. Ly, D. Echeverria, M.R. Hassler, B.M.D.C. Godinho, M. Nikan, A. Khvorova, Hydrophobicity drives the systemic distribution of lipid-conjugated siRNAs via lipid transport pathways, Nucleic Acids Res. 47 (2019) 1070–1081. https://doi.org/10.1093/nar/gky1232.

[94] M.R. Hassler, A.A. Turanov, J.F. Alterman, R.A. Haraszti, A.H. Coles, M.F. Osborn, D. Echeverria, M. Nikan, W.E. Salomon, L. Roux, B.M.D.C. Godinho, S.M. Davis, D. V. Morrissey, P.D. Zamore, S. Ananth Karumanchi, M.J. Moore, N. Aronin, A. Khvorova,

Comparison of partially and fully chemically-modified siRNA in conjugate-mediated delivery in vivo, Nucleic Acids Res. 46 (2018) 2185–2196. https://doi.org/10.1093/nar/gky037.

[95] R.A. Haraszti, L. Roux, A.H. Coles, A.A. Turanov, J.F. Alterman, D. Echeverria, B.M.D.C. Godinho, N. Aronin, A. Khvorova, 5'-Vinylphosphonate improves tissue accumulation and efficacy of conjugated siRNAs in vivo, Nucleic Acids Res. 45 (2017) 7581–7592. https://doi.org/10.1093/nar/gkx507.

[96] K. Nishina, T. Unno, Y. Uno, T. Kubodera, T. Kanouchi, H. Mizusawa, T. Yokota, Efficient in vivo delivery of siRNA to the liver by conjugation of α-tocopherol, Molecular Therapy. 16 (2008) 734–740. https://doi.org/10.1038/mt.2008.14.

[97] C. Wolfrum, S. Shi, K.N. Jayaprakash, M. Jayaraman, G. Wang, R.K. Pandey, K.G. Rajeev, T. Nakayama, K. Charrise, E.M. Ndungo, T. Zimmermann, V. Koteliansky, M. Manoharan, M. Stoffel, Mechanisms and optimization of in vivo delivery of lipophilic siRNAs, Nat Biotechnol. 25 (2007) 1149–1157. https://doi.org/10.1038/nbt1339.

[98] K.M. Brown, J.K. Nair, M.M. Janas, Y.I. Anglero-Rodriguez, L.T.H. Dang, H. Peng, C.S. Theile, E. Castellanos-Rizaldos, C. Brown, D. Foster, J. Kurz, J. Allen, R. Maganti, J. Li, S. Matsuda, M. Stricos, T. Chickering, M. Jung, K. Wassarman, J. Rollins, L. Woods, A. Kelin, D.C. Guenther, M.W. Mobley, J. Petrulis, R. McDougall, T. Racie, J. Bombardier, D. Cha, S. Agarwal, L. Johnson, Y. Jiang, S. Lentini, J. Gilbert, T. Nguyen, S. Chigas, S. LeBlanc, U. Poreci, A. Kasper, A.B. Rogers, S. Chong, W. Davis, J.E. Sutherland, A. Castoreno, S. Milstein, M.K. Schlegel, I. Zlatev, K. Charisse, M. Keating, M. Manoharan, K. Fitzgerald, J.-T. Wu, M.A. Maier, V. Jadhav, Expanding RNAi therapeutics to extrahepatic tissues with lipophilic conjugates, Nat Biotechnol. 40 (2022) 1500–1508. https://doi.org/10.1038/s41587-022-01334-x.

[99] S.M. Sarett, T.A. Werfel, L. Lee, M.A. Jackson, K. V. Kilchrist, D. Brantley-Sieders, C.L. Duvall, Lipophilic siRNA targets albumin in situ and promotes bioavailability, tumor penetration, and carrier-free gene silencing, Proc Natl Acad Sci U S A. 114 (2017) E6490–E6497. https://doi.org/10.1073/pnas.1621240114.

[100] I. V. Chernikov, D. V. Gladkikh, U.A. Karelina, M.I. Meschaninova, A.G. Ven'yaminova, V. V. Vlassov, E.L. Chernolovskaya, Trimeric Small Interfering RNAs and Their Cholesterol-Containing Conjugates Exhibit Improved Accumulation in Tumors, but Dramatically Reduced Silencing Activity, Molecules. 25 (2020) 1877. https://doi.org/10.3390/molecules25081877.

[101] I. V. Chernikov, D. V. Gladkikh, M.I. Meschaninova, A.G. Ven'yaminova, M.A. Zenkova, V. V. Vlassov, E.L. Chernolovskaya, Cholesterol-Containing Nuclease-Resistant siRNA Accumulates in Tumors in a Carrier-free Mode and Silences MDR1 Gene, Mol Ther Nucleic Acids. 6 (2017) 209–220. https://doi.org/10.1016/j.omtn.2016.12.011.

[102] X. Yang, A.K. Lyer, A. Singh, E. Choy, F.J. Hornicek, M.M. Amiji, Z. Duan, MDR1 siRNA loaded hyaluronic acid-based CD44 targeted nanoparticle systems circumvent paclitaxel resistance in ovarian cancer, Sci Rep. 5 (2015) 1–9. https://doi.org/10.1038/srep08509.

[103] S. Yadav, L.E. Van Vlerken, S.R. Little, M.M. Amiji, Evaluations of combination MDR-1 gene silencing and paclitaxel administration in biodegradable polymeric nanoparticle formulations to overcome multidrug resistance in cancer cells, Cancer Chemother Pharmacol. 63 (2009) 711–722. https://doi.org/10.1007/s00280-008-0790-y.

[104] W. Liu, Y.L. Lo, C. Hsu, Y.T. Wu, Z.X. Liao, W.J. Wu, Y.J. Chen, C. Kao, C.C. Chiu, L.F. Wang, CS-PEI/Beclin-siRNA Downregulate Multidrug Resistance Proteins and Increase Paclitaxel Therapeutic Efficacy against NSCLC, Mol Ther Nucleic Acids. 17 (2019) 477–490. https://doi.org/10.1016/j.omtn.2019.06.017.

[105] M.F. Osborn, A.H. Coles, D. Golebiowski, D. Echeverria, M.P. Moazami, J.K. Watts, M. Sena-Esteves, A. Khvorova, Efficient gene silencing in brain tumors with hydrophobically modified siRNAs, Mol Cancer Ther. 17 (2018) 1251–1258. https://doi.org/10.1158/1535-7163.MCT-17-1144.

[106] S. Sakamoto, S. Schwarze, N. Kyprianou, Anoikis disruption of focal adhesion-Akt signaling impairs renal cell carcinoma, Eur Urol. 59 (2011) 734–744. https://doi.org/10.1016/j.eururo.2010.12.038.

[107] M.S. Park, B.R. Kim, S.M. Dong, S.H. Lee, D.Y. Kim, S.B. Rho, The antihypertension drug doxazosin inhibits tumor growth and angiogenesis by decreasing VEGFR-2/Akt/mTOR signaling and VEGF and HIF-1α expression, Oncotarget. 5 (2014) 4935–4944. https://doi.org/10.18632/oncotarget.2064.

[108] O.P. Joffre, E. Segura, A. Savina, S. Amigorena, Cross-presentation by dendritic cells, Nat Rev Immunol. 12 (2012) 557–569. https://doi.org/10.1038/nri3254.

[109] M. Gros, S. Amigorena, Regulation of antigen export to the cytosol during cross-presentation, Front Immunol. 10 (2019) 41. https://doi.org/10.3389/fimmu.2019.00041.

[110] R. van der Meel, E. Sulheim, Y. Shi, F. Kiessling, W.J.M. Mulder, T. Lammers, Smart cancer nanomedicine, Nat Nanotechnol. 14 (2019) 1007–1017. https://doi.org/10.1038/s41565-019-0567-y.

[111] K. Raemdonck, B. Naeye, A. Høgset, J. Demeester, S.C. De Smedt, Prolonged gene silencing by combining siRNA nanogels and photochemical internalization, Journal of Controlled Release. 145 (2010) 281–288. https://doi.org/10.1016/j.jconrel.2010.04.012.

[112] B. Naeye, K. Raemdonck, K. Remaut, B. Sproat, J. Demeester, S.C. De Smedt, PEGylation of biodegradable dextran nanogels for siRNA delivery, European Journal of Pharmaceutical Sciences. 40 (2010). https://doi.org/10.1016/j.ejps.2010.04.010.

[113] B. Naeye, H. Deschout, M. Röding, M. Rudemo, J. Delanghe, K. Devreese, J. Demeester, K. Braeckmans, S.C. De Smedt, K. Raemdonck, Hemocompatibility of siRNA loaded dextran nanogels, Biomaterials. 32 (2011). https://doi.org/10.1016/j.biomaterials.2011.08.015.

[114] G.R. Dakwar, E. Zagato, J. Delanghe, S. Hobel, A. Aigner, H. Denys, K. Braeckmans, W. Ceelen, S.C. De Smedt, K. Remaut, Colloidal stability of nano-sized particles in the peritoneal fluid: Towards optimizing drug delivery systems for intraperitoneal therapy, Acta Biomater. 10 (2014) 2965–2975. https://doi.org/10.1016/J.ACTBIO.2014.03.012.

[115] J.C. Fraire, G. Houthaeve, J. Liu, L. Raes, L. Vermeulen, S. Stremersch, T. Brans, G. García-Díaz Barriga, S. De Keulenaer, F. Van Nieuwerburgh, R. De Rycke, J. Vandesompele, P. Mestdagh, K. Raemdonck, W.H. De Vos, S. De Smedt, K. Braeckmans, Vapor nanobubble is the more reliable photothermal mechanism for inducing endosomal escape of siRNA without disturbing cell homeostasis, Journal of Controlled Release. 319 (2020) 262–275. https://doi.org/10.1016/j.jconrel.2019.12.050.

[116] P. Merckx, L. De Backer, L. Van Hoecke, R. Guagliardo, M. Echaide, P. Baatsen, B. Olmeda, X. Saelens, J. Pérez-Gil, S.C. De Smedt, K. Raemdonck, Surfactant protein B (SP-B) enhances the cellular siRNA delivery of proteolipid coated nanogels for inhalation therapy, Acta Biomater. 78 (2018) 236–246. https://doi.org/10.1016/j.actbio.2018.08.012.